

อิพ็อกซี/ซิลิกาคัดแปรด้วยแอมิโน/เพอร์ฟลูออโรออกทิลไทรเอทอกซีไซเลนนาโนคอมพอสิต
สำหรับการเคลือบไฮบริดซ่อมแซมตัวเอง



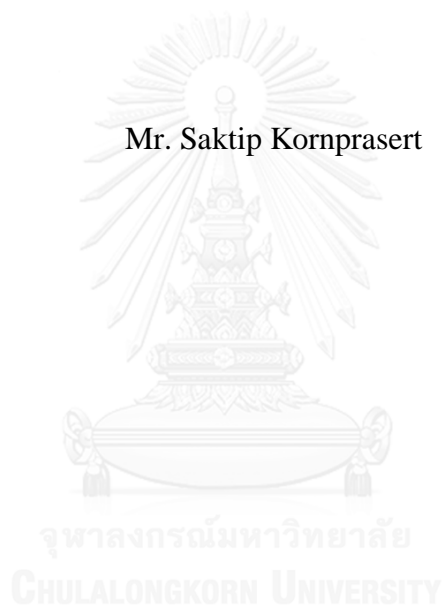
บทคัดย่อและแฟ้มข้อมูลฉบับเต็มของวิทยานิพนธ์ตั้งแต่ปีการศึกษา 2554 ที่ให้บริการในคลังปัญญาจุฬาฯ (CUIR)
เป็นแฟ้มข้อมูลของนิสิตเจ้าของวิทยานิพนธ์ ที่ส่งผ่านทางบัณฑิตวิทยาลัย

The abstract and full text of theses from the academic year 2011 in Chulalongkorn University Intellectual Repository (CUIR)
are the thesis authors' files submitted through the University Graduate School.

วิทยานิพนธ์นี้เป็นส่วนหนึ่งของการศึกษาตามหลักสูตรปริญญาวิทยาศาสตรมหาบัณฑิต
สาขาวิชาปิโตรเคมีและวิทยาศาสตร์พอลิเมอร์
คณะวิทยาศาสตร์ จุฬาลงกรณ์มหาวิทยาลัย
ปีการศึกษา 2558
ลิขสิทธิ์ของจุฬาลงกรณ์มหาวิทยาลัย

EPOXY/AMINO-
MODIFIED SILICA/PERFLUOROCTYL TRIETHOXYSILANE
NANOCOMPOSITE FOR SELF-HEALING HYBRID COATING

Mr. Saktip Kornprasert



A Thesis Submitted in Partial Fulfillment of the Requirements
for the Degree of Master of Science Program in Petrochemistry and Polymer Science
Faculty of Science
Chulalongkorn University
Academic Year 2015
Copyright of Chulalongkorn University

Thesis Title EPOXY/AMINO-MODIFIED
SILICA/PERFLUOROCTYL
TRIETHOXYSILANE NANOCOMPOSITE
FOR SELF-HEALING HYBRID COATING

By Mr. Saktip Kornprasert

Field of Study Petrochemistry and Polymer Science

Thesis Advisor Professor Pattarapan Prasassarakich, Ph.D.

Thesis Co-Advisor Assistant Professor Suwadee Kongparakul, Ph.D.

Accepted by the Faculty of Science, Chulalongkorn University in Partial
Fulfillment of the Requirements for the Master's Degree

..... Dean of the Faculty of Science
(Associate Professor Polkit Sangvanich, Ph.D.)

THESIS COMMITTEE

..... Chairman
(Assistant Professor Warinthorn Chavasiri, Ph.D.)

..... Thesis Advisor
(Professor Pattarapan Prasassarakich, Ph.D.)

..... Thesis Co-Advisor
(Assistant Professor Suwadee Kongparakul, Ph.D.)

..... Examiner
(Associate Professor Nuanphun Chantarasiri, Ph.D.)

..... External Examiner
(Assistant Professor Sutha Sutthiruangwong, Ph.D.)

ศักดิ์ทิพย์ กรประเสริฐ : อีพ็อกซี/ซิลิกาคัดแปรด้วยเอมิโน/เพอร์ฟลูออโรออกทิลไทรเอทอกซีไฮเลนนาโนคอมพอสิตสำหรับการเคลือบไฮบริดซ่อมแซมตัวเอง (EPOXY/AMINO-MODIFIED SILICA/PERFLUOROCTYL TRIETHOXSILANE NANOCOMPOSITE FOR SELF-HEALING HYBRID COATING) อ.ที่ปรึกษาวิทยานิพนธ์หลัก: ศ. ดร.ภัทรพรรณ ประศาสน์สารกิจ, อ.ที่ปรึกษาวิทยานิพนธ์ร่วม: ผศ. ดร.สุวดี ก้องพารากุล, 79 หน้า.

งานวิจัยนี้เป็นการศึกษาการสังเคราะห์นาโนคอมพอสิตของอีพ็อกซี ซิลิกาคัดแปรพื้นผิวและสารช่วยรักษาตัวเองสำหรับการใช้ป้องกันการกัดกร่อนของเหล็กกล้า 3-โกลซีดอกซีโพรพิลไตรเมทอกซีไซเรน (GPTMS) และ 3-อะมิโนโพรพิลไตรเอทอกซีไฮเลน (APTES) ถูกใช้ในการคัดแปรพื้นผิวของซิลิกาเพื่อเพิ่มความสามารถในการกระจายตัวอย่างสม่ำเสมอในพอลิเมอร์เมทริกซ์ นอกจากนี้ยังได้ศึกษาการนำเพอร์ฟลูออโรออกทิลไทรเอทอกซีไฮเลน เอทานอลามีนและไดเอทานอลามีนซึ่งเป็นสารช่วยรักษาตัวเองที่ถูกแอนแคปซูลด้วยพอลิเมอร์มาใช้ร่วมกับซิลิกาที่ถูกคัดแปรพื้นผิวเพื่อสร้างฟิล์มเคลือบผิวป้องกันการกัดกร่อนที่เกิดจากสารอินทรีย์ร่วมกับสารอนินทรีย์บนพื้นผิวของโลหะตัวอย่าง งานวิจัยนี้ได้ศึกษาผลของชนิดของสารช่วยทำให้แข็ง ปริมาณซิลิกาคัดแปรพื้นผิวและปริมาณของสารช่วยรักษาตัวเองที่ส่งต่อประสิทธิภาพการป้องกันการกัดกร่อนของคอมพอสิต ซิลิกาคัดแปรพื้นผิวและสารช่วยรักษาตัวเองถูกวิเคราะห์ด้วยเครื่องฟูเรียรทรานฟอร์มอินฟราเรดสเปกโตรสโคปี กล้องจุลทรรศน์แบบใช้แสงถูกใช้ในการศึกษาโครงสร้างอสัณฐานและลักษณะการกระจายตัวของซิลิกาคัดแปรพื้นผิวในนาโนคอมพอสิต ประสิทธิภาพในการป้องกันการกัดกร่อนของฟิล์มที่เคลือบบนแผ่นเหล็กถูกศึกษาด้วยวิธีทาเฟลพล็อต ไซคลิกโวลแทมเมตรี และการทดสอบความทนละอองน้ำเกลือพบว่าเหล็กที่เคลือบด้วย epoxy/3wt%GMS/20wt%POT มีประสิทธิภาพในการป้องกันการกัดกร่อนมากที่สุด (ค่ากระแสไฟฟ้าการกัดกร่อนเท่ากับ 0.012 mA/cm^2 และมีอัตราการกัดกร่อนต่อปีเท่ากับ 0.139 มิลลิเมตรต่อปี โดยผลการศึกษาทางไฟฟ้าเคมีมีความสอดคล้องกับผลการศึกษาออสัณฐานวิทยาจากกล้องจุลทรรศน์แบบใช้แสงและกล้องจุลทรรศน์อิเล็กตรอนแบบส่องกราด

สาขาวิชา ปีโตรเคมีและวิทยาศาสตร์พอลิเมอร์ ลายมือชื่อนิติต

ปีการศึกษา 2558

ลายมือชื่อ อ.ที่ปรึกษาหลัก

ลายมือชื่อ อ.ที่ปรึกษาร่วม

5672256123 : MAJOR PETROCHEMISTRY AND POLYMER SCIENCE

KEYWORDS: NANOCOMPOSITE COATING / NANO-SILICA / CORROSION / EPOXY COATING / SELF-HEALING

SAKTIP KORNPRASERT: EPOXY/AMINO-MODIFIED SILICA/PERFLUOROOCXYL TRIETHOXYSILANE NANOCOMPOSITE FOR SELF-HEALING HYBRID COATING. ADVISOR: PROF. PATTARAPAN PRASASSARAKICH, Ph.D., CO-ADVISOR: ASST. PROF. SUWADEE KONGPARAKUL, Ph.D., 79 pp.

Self-healing hybrid nanocomposite was successfully prepared from epoxy resin containing self-healing microcapsules and modified nano-silica as a reinforcement to enhance anticorrosion performance of epoxy coating. 3-Glycidoxypropyl-trimethoxysilane (GPTMS) and 3-aminopropyl-trimethoxysilane (APTES) were used to modify nano-silica surface in order to accomplish proper dispersion of nanoparticles in polymer matrix. Perfluorooctyl triethoxysilane (POT), Ethanolamine (ETA) and Diethanolamine (DEA) as self-healing agents were encapsulated by polymer shell and incorporated into the epoxy coating along with modified nano-silica to form anticorrosion barrier of organic and inorganic coating on a cold-rolled steel (CRS) substrate. The effect of epoxy curing agents, modified silica and self-healing loading on the anticorrosion properties were studied. The modified silica nanoparticles and the self-healing agents were characterized using Fourier transform infrared spectroscopy (FTIR). Optical microscope (OM) was used to observe the microstructure and dispersion of nanoparticles. Anticorrosion performance of the coated CRS specimens was investigated by Tafel plot, cyclic voltammetry (CV) and salt spray test. The epoxy/3wt%GMS/20wt%POT nanocomposite possessed the best corrosion performance ($I_{\text{corr}} = 0.012 \text{ mA/cm}^2$ and corrosion rate of 0.139 mm/year). Electrochemical results were in agreement with the morphological results obtained from optical microscopy and scanning electron microscopy (SEM)

Field of Study: Petrochemistry and
Polymer Science

Academic Year: 2015

Student's Signature

Advisor's Signature

Co-Advisor's Signature

ACKNOWLEDGEMENTS

The author would like to express heartfelt gratitude and sincere appreciation to his advisor, Prof. Dr. Pattarapan Prasassarakich and co-advisor, Asst. Prof. Suwadee Kongparakul for the encouraging guidance, helpful discussion, supervision, and support throughout this research. The author also would like to acknowledge Asst. Prof. Warinthorn Chavasiri, Assoc. Prof. Nuanphun Chantarasiri and Asst. Prof. Sutha Sutthiruangwong for serving as the dissertation chairman and members of the thesis committee, respectively, and for their worthy comments and suggestions.

The author gratefully acknowledges the funding support from the Thailand Research Fund under contract no. TRG5780172 and National Research University (NRU).

Many thanks also go to the Petrochemistry and Polymer Science Program, Faculty of Science, Chulalongkorn University, Department of Chemical Technology, Faculty of Science, Chulalongkorn University and Department of Chemistry, Faculty of Science and Technology, Thammasat University for providing research facilities throughout this research work.

Finally, the author also expresses his deep appreciation to his family for their love, support and endless encouragement throughout his entire study.

CONTENTS

	Page
THAI ABSTRACT	iv
ENGLISH ABSTRACT.....	v
ACKNOWLEDGEMENTS	vi
CONTENTS.....	vii
LIST OF TABLE	x
LIST OF FIGURES	xi
LIST OF ABBREVIATIONS.....	1
CHAPTER I.....	2
INTRODUCTION	2
1.1 The Purpose of the Investigation	2
1.2 The Objective.....	3
1.3 Scope of the Investigation.....	3
CHAPTER II.....	4
THEORY AND LITERATURE REVIEW	4
2.1 Epoxy Resin.....	4
2.2 Synthesis of Epoxy Polymer.....	6
2.3 Silica Surface Modification	11
2.4 Epoxy/Silica Nanocomposite.....	14
2.5 Characterization of Epoxy/Silica Nanocomposite	17
2.6 Corrosion	19
2.6.1 Types of Corrosion.....	22
2.6.2 Corrosion Prevention.....	23
2.7 Self-Healing Materials.....	24
2.8 Literature Reviews	26
CHAPTER III	30
EXPERIMENTAL.....	30
3.1 Chemicals.....	30
3.2 Equipments	30

	Page
3.3 Synthesis of Modified Silica Nanoparticles.....	31
3.3.1 APTES-modified Silica.....	31
3.3.2 GPTES-modified Silica.....	32
3.4 Synthesis of Self-Healing Microcapsules	32
3.4.1 Synthesis of Perfluorooctyltriethoxysilane (POT) Loaded Microcapsules	32
3.4.2 Synthesis of Amine Loaded Microcapsules	33
3.5 Coating of Epoxy Nanocomposite on Steel Samples	37
3.6 Characterization Methods	38
3.6.1 Fourier Transform Infrared (FT-IR) Spectroscopy	38
3.6.2 Study of Dispersion of Silica.....	38
3.6.3 Contact angle Measurement	38
3.6.4 Morphological Study.....	39
3.6.5 Cyclic Voltammetry	39
3.6.6 Corrosion Study.....	40
CHAPTER IV	42
RESULTS AND DISCUSSION	42
4.1 Synthesis of Modified Silica Nanoparticles via Sol-gel Reaction.....	42
4.2 Modification of Silica Nanoparticles.....	46
4.3 Synthesis of Self-Healing Microcapsules	47
4.3.1 Synthesis of POT Loaded Microcapsules	47
4.3.2 Synthesis of Amine Loaded Microcapsules	48
4.4 Characterization of Self-Healing Hybrid Nanocomposite.....	50
4.5 Dispersion of Silica Nanoparticles in Epoxy Composite.....	52
4.5.1 Effect of Curing Agents	52
4.5.2 Effect of Silica.....	52
4.6 Corrosion Studies.....	55
4.6.1 Effect of Self-healing Agent.....	55
4.6.2 Effect of Silica Loading and Curing Agents	57

	Page
4.7 Salt Spray Test	62
4.8 Morphology of Epoxy/Modified silica/Self-Healing Nanocomposite on Steel	64
CHAPTER V	66
CONCLUSIONS AND SUGGESTIONS.....	66
5.1 Conclusions.....	66
5.2 Suggestions of the Future Work	67
REFERENCES	68
APPENDIX.....	71
Appendix A.....	72
Appendix B.....	76
Appendix C.....	78
VITA.....	79



LIST OF TABLE

Table	Page
2.1 Commercial curing agents	10
2.2 Typical silane coupling agents used in the preparation of hybrid silica-polymer materials.....	13
4.1 The amount of amine groups obtained by direct titration and TGA.....	46
4.2 Amount on silica conversion, solid content, average particle size (\bar{D}_n) and particles size distribution (PSD) of amines encapsulated in polystyrene shell.....	49
4.3 Corrosion potential (E_{corr}), corrosion current (I_{corr}), corrosion rate (CR) and % corrosion rate values calculated from Tafel plots for epoxy/modified silica/self-healing nanocomposite samples in 1.0 M H_2SO_4 solution.....	55
4.4 Corrosion potential (E_{corr}), corrosion current (I_{corr}), corrosion rate (CR) and % corrosion rate values calculated from Tafel plots for epoxy/modified silica nanocomposite and epoxy/modified silica/self-healing nanocomposite samples in 1M H_2SO_4 solution.....	60
4.5 Rating of failure according to ASTM 1654.....	61

LIST OF FIGURES

Figure	Page
2.1 Chemical structure of bisphenol A based epoxy resins.....	3
2.2 Chemical structure of bisphenol F based epoxy resins	4
2.3 Chemical structure of hydantoin resins.....	4
2.4 Chemical structure of Novolacs.....	4
2.5 Chemical structure of peracid resins.....	5
2.6 Chemical structure of bisphenol-A and epichlorohydrin.....	6
2.7 Molecular structures of (a) bisphenol-A type epoxy resin (b) Novolac epoxy resins (c) glycidyl ester resins.....	7
2.8 Surface modification of silica nanoparticles.....	12
2.9 Functionalization of silica nanoparticles.....	12
2.10 Scheme of surface modification for nano-size filler.....	15
2.11 Wettability illustrated by examples of contact angles and spreading.....	17
2.12 Combined anodic and cathodic Tafel plots.....	17
2.13 The formation of rust in iron via electrochemical reaction.....	21
2.14 Types of corrosion: (a) Galvanic corrosion, (b) Concentration cell corrosion, (c) Pitting, (d) Stress corrosion cracking, (e) Intergranular corrosion and (f) Uniform corrosion attacks.....	22
2.15 Illustration of the capsule-based sealing approach.....	24
3.1 The schematic diagram of AMS and GMS synthesis.....	33
3.2 The preparation of perfluorooctyl triethoxysilane encapsulated in polymeric microcapsules.....	34
3.3 The preparation of amines loaded microcapsules.....	35
3.4 (a) Spray gun and (b) Steel coupons coated by spray method.....	36
3.5 The electrochemical Tafel slope analysis apparatus.....	40
4.1 TEM images of amino-modified silica synthesized via sol-gel reation (a) 180,000X and (b) 200,000X.....	43
4.2 (a) TGA and (b) DTG curve of amino-modified silica nanoparticle with various APTES loading.....	44

Figure	Page
4.3 TEM images of APTES-modified silica nanoparticles at (a) 180,000X (b) 220,000X and GPTMS-modified silica nanoparticles at (c) 180,000X (d) 220,000X	45
4.4 Particle size distribution of (a) AMS and (b) GMS.....	46
4.5 Transmission electron micrograph of POT encapsulated in PUF microcapsules containing.....	48
4.6 Histograms of particle size distribution of (a) seed core latex (b) ETA/PS and (c) DEA/PS.....	48
4.7 FTIR spectra of (a) untreated nano-silica (b) AMS and (c) GMS.....	50
4.8 FTIR spectra of (a) POT and (b) amines encapsulated in polymer shell.....	50
4.9 Effect of curing agent on nanocomposite (TEPA as curing agent) with (a) 3wt%AMS and (b) 3wt%GMS and nanocompostie (<i>p</i> -PDA as curing agent) with (c) 3wt%AMS and (d) 3wt%GMS (magnification of 40X).....	52
4.10 Effect of untreated silica loading on the dipersion of silica on 3wt% untreated Si/epoxy (a) 40X, (a') 200X and 5wt% untreated Si/epoxy (b) 40X, (b') 200X (<i>p</i> -PDA as curing agent).....	52
4.11 Effect of modified silica loading on the dipersion of silica (a) 3wt% AMS/epoxy, (b) 5wt%AMS/epoxy, (c) 3wt% GMS/epoxy, (d)5wt%GMS/epoxy (at the magnification of 40X) (a', b', c', d' showed magnification at 200X)(<i>p</i> -PDA as curing agent).....	54
4.13 Cyclic voltammetry (a) and Tafel plot and (b) of epoxy/modified silica/self-healing nanocomposite with variuos type of self- healing microcapsule.....	55
4.14 Cyclic voltammetry of epoxy nanocomposite with (a) various type of silica (b) various amount of silica in TEPA-epoxy (c) various amount of silica in <i>p</i> -PDA –epoxy and (d) various amount of POT microcapsules.....	57

Figure	Page
4.15 Scanning Tafel plots for epoxy nanocomposite with (a) various type of silica (b) various amount of silica in TEPA-epoxy (c) various amount of silica in <i>p</i> -PDA –epoxy and (d) various amount of POT microcapsules.....	58
4.16 Corrosion rate of neat epoxy and epoxy/silica nanocomposite with various types of curing agents and POT loading at 10 and 20 wt%.....	60
4.17 Coupons of coated steel of epoxy/modified silica/self-healing nanocomposite coating after salt spray test for 0, 24, 48 72 and 96h; <i>p</i> -PDA-epoxy/3wt%GMS nanocomposite with the incorporate of (a) 5wt% POT,(b) 10wt% POT, (c) 15wt% POT, (d) 20wt%POT and <i>p</i> -PDA-epoxy incorporate with (e) 1wt% GMS, (f) 2wt%GMS, (g) 3wt% GMS , (h) 4wt% GMS and (i) 5wt%GMS.....	62
4.18 SEM images of surface area of (a) epoxy/3wt%GMS/20%POT and (b) epoxy/3wt%GMS/20%DEA nanocomposite coating (50 μ m thickness) before corrosion test, (a') and (b') showed nanocomposite coating after corrosion test (180X magnification).....	64
4.19 Self-healing mechanism of epoxy/GMS/POT coatings; (a) before exposed in corrosive environment, (b) during corrosion process and (c) new film layer obtained by POT.....	64

LIST OF ABBREVIATIONS

APS	:	Ammonium persulfate
APTES	:	(3-Aminopropyl)triethoxysilane
BA	:	Butyl acrylate
CR	:	Corrosion rate
CV	:	Cyclic voltammogram
DEA	:	Diethanolamine
DGEBA	:	Diglycidyl ether of bisphenol A
\bar{D}_n	:	Mean number diameter (average particle size)
E_{corr}	:	Corrosion potential
ETA	:	Ethanolamine
FTIR	:	Fourier transform infrared spectroscopy
GPTMS	:	(3-Glycidyloxypropyl)trimethoxysilane
I_{corr}	:	Corrosion current
MA	:	Methacrylic acid
MMA	:	Methyl methacrylate
<i>p</i> -PDA	:	<i>p</i> -Phenylenediamine
POT	:	Perfluorooctyltriethoxysilane
PSD	:	Particle size distribution
SEM	:	Scanning electron microscopy
TEM	:	Transmission electron microscopy
TEPA	:	Tetraethylenepentadamine
TGA	:	Thermogravimetric analysis

CHAPTER I

INTRODUCTION

1.1 The Purpose of the Investigation

Corrosion is the most concern problem which encounters with the material failure, equipment shutdown, waste of valuable resources, loss or contamination of product, reduction in efficiency and usually expensive to repair. The efforts to develop more efficient methods to prevent corrosion have been ongoing throughout this century. Anticorrosion approaches commonly used to slow down the corrosion rate are protective coating, cathodic protection and addition of inhibitors. Surface coating is one of the most potential method for anticorrosion of metal. It can conventionally isolate metal surface from the corrosive media. Therefore, many chemicals were used to study on anticorrosion coating.

Epoxy polymer has become an attractive subject of investigation for surface coating. It processes many suitable properties such as mechanical properties, thermal properties, high chemical resistance and outstanding adhesion to various substrates. Epoxy has a wide range of applications, including electronic components, coatings, adhesives and composite materials [1]. However, in terms of coating applications, epoxy polymer still have some drawback such as brittle and notch sensitive [2]. As a result, tremendous effort has been focused on toughness improvement. The addition of silica nanoparticles has makes epoxy into hybrid nanocomposite which could enhance mechanical properties, thermal stability and anticorrosive performance. The modified silica nanoparticles with organosilane could be compatible with polymers and give a good dispersion [3]. Furthermore, a different type of hardener can affect film properties including mechanical and thermal properties. Besides improvement of anticorrosion property by hybrid nanocomposite, the self-healing ability is a particularly vital property for coatings designed to protect the material against corrosion. The encapsulation of corrosion inhibitors and the

introduction of the capsules into the matrix of the coating are considered [4]. Therefore, type of hardener and modified silica nanoparticles were investigated to find the types and optimum amount added to achieve best anticorrosion performance.

In the research work, epoxy/modified silica/self-healing hybrid nanocomposite were synthesized and prepared. The anticorrosive properties of epoxy/modified silica/self-healing hybrid nanocomposite on cold-rolled steel were studied.

1.2 The Objective

The objectives of thesis can be summarized as follows:

1. To prepare epoxy/modified silica/self-healing nanocomposite for self-healing hybrid coating
2. To study the effects of modified silica and self-healing agents loading on the anticorrosive properties of nanocomposite.

1.3 Scope of the Investigation

The experimental procedure for this research was presented as follows:

1. Literature survey study for this research work.
2. To prepare modified nanosilica and self-healing agents.
3. To prepare the self-healing hybrid nanocomposite and study the effects of modified nanosilica loading at 1-5 wt% and self-healing agent loading at 10 wt%.
4. To characterize the self-healing hybrid nanocomposite by Fourier transform infrared, thermogravimetric analysis and optical microscopy.
5. To investigate the anticorrosion properties and morphology of the self-healing hybrid nanocomposite.

CHAPTER II

THEORY AND LITERATURE REVIEW

2.1 Epoxy Resin [1]

Epoxy resins were first commercialized in 1946 and are widely used in industry as protective coatings and for structural applications, such as laminates and composite, tooling, molding, casting, bonding and adhesives, and others [3]. Epoxy resin is the collective name for compounds that contain two or more epoxy groups in its molecules and is able to form three-dimensional network structure solidifying under suitable chemical reagent. Various properties over a wide range at an acceptable cost could be achieved depending on the type of epoxy and hardener used. The epoxy resin has excellent adhesion, chemical and heat resistance, mechanical properties and insulating properties. However, in terms of structural applications, epoxy resins are usually brittle and notch [5]. It is also possible to improve epoxy resins properties by choosing different epoxy oligomer and hardener or suitable modification method. Therefore, it has become one of the most popular thermosetting resins in industrial applications. Some commercial epoxy resins and examples of important hardener are discussed below.

Commercial types of epoxy resins

Diglycidyl ether of bisphenol A

The most widely used epoxy resins are diglycidyl ethers of bisphenol A, DGEBA (Figure 2.1). These are produced by the reaction of bisphenol A and epichlorohydrin in the presence of sodium hydroxide.

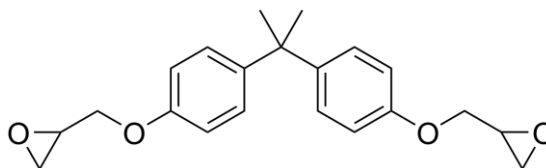


Figure 2.1 Chemical structure of bisphenol A based epoxy resins [5]

Bisphenol F based epoxy resins

Instead of reacting bisphenol A with epichlorohydrin to form a liquid resin, a similar reaction can be conducted between bisphenol F and epichlorohydrin. Figure 2.2 shows the chemical structure of bisphenol F based epoxy resins.

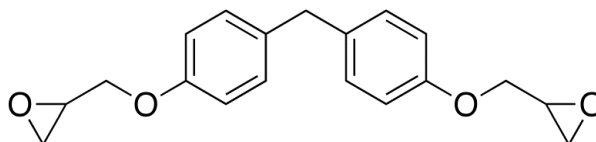


Figure 2.2 Chemical structure of bisphenol F based epoxy resins [5]

Hydantoin resins

In recent years, the hydantoin resins (Figure 2.3) have shown greater popularity for increasing temperature resistance and improving mechanical properties, particularly in structural composite. However, this type of epoxy has presented toxicity problems. At least one hydantoin based product is being supplied for commercial applications, but it requires special handling precautions.

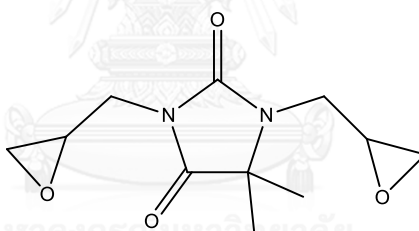


Figure 2.3 Chemical structure of hydantoin resins [5]

Novolacs

Novolacs are epoxidized phenol-formaldehyde or substituted phenol-formaldehyde resins. Chemical structure of Novolacs is shown in Figure 2.4.

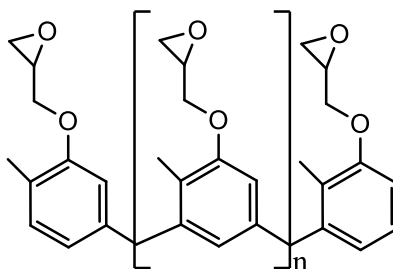


Figure 2.4 Chemical structure of Novolacs [5]

Peracid resins

On the peracid resins, the cyclic types contribute to higher crosslink densities. These resins have lower viscosities and color compared to novolac and DGEBA types. Such a typical resin is illustrated by the structure of 3,4-epoxycyclohexylmethyl-3,4-epoxycyclohexane carboxylate as shown in Figure 2.5.

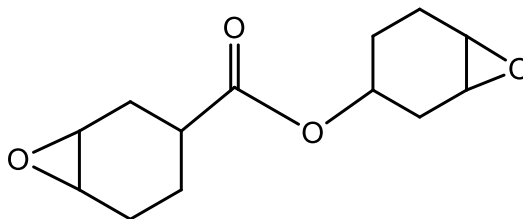


Figure 2.5 Chemical structure of peracid resins [5]

2.2 Synthesis of Epoxy Polymer [6]

Epoxy resins can be divided into glycidyl epoxy resins and non-glycidyl epoxy resins, according to their synthesis methods. The glycidyl epoxy resins are formed by a condensation reaction of appropriate dihydroxy compound, dibasic acid or a diamine and epichlorohydrin, whereas the non-glycidyl epoxy resins are prepared by peroxidation of olefinic double bond. According to the synthesis methods, glycidyl ether resin, glycidyl ester resin and glycidyl amine resin belong to glycidyl resins, whereas alicyclic epoxy resin and aliphatic epoxy resin are classified into non-glycidyl epoxy resins. Moreover, glycidyl ether epoxy resin can be further divided into diglycidyl ether of bisphenol-A (DGEBA) and Novolac epoxy resin. Both of DGEBA and Novolac epoxy resins are the most commonly used resins in industrial applications. DGEBA epoxy resins are produced from reactions between epichlorohydrin and bisphenol-A as shown in Figures 2.6. The property of molecular structure of this epoxy resin is that the molecular chain contains active epoxy groups. Because there are active epoxy groups in the molecular chain, the epoxy resin is able to have cross linking reactions with hardeners to form 3D crosslinked polymer network.

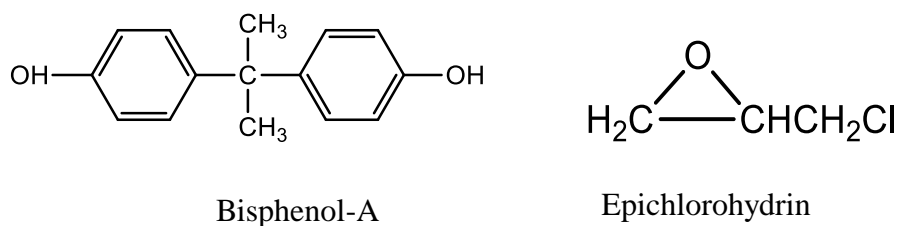


Figure 2.6 Chemical structure of bisphenol-A and epichlorohydrin [6]

Novolac epoxy resins are formed under a reaction between phenolic Novolac resin and epichlorohydrin. Comparing with DGEBA, Novolac epoxy resins contain more than two epoxy groups in its molecular structure. Thus, its curing products have larger cross linking density, better thermal stability, mechanical properties, dielectric properties, and water and corrosion resistance. As a result, they are widely used to make microelectronic molding compounds. Glycidyl ester resins have better dielectric properties and weather resistance. Their viscosity is normally lower than other epoxy resins. Glycidyl ester resins are more adhesive than other epoxy resins, thus their condensates have better mechanical properties. Moreover, they also have good resistance to very low temperature, which means that their adhesive strength is still higher than other epoxy resins at very low temperature.

Glycidyl amine resins, on the other hand, have high epoxide equivalent, big cross-linking density and higher thermal resistance. Thus, they have been used to manufacture carbon fibre reinforced plastics (CFRP). Alicyclic epoxy resins are prepared by epoxidation of alicyclic alkene and their molecular structure has a large difference comparing with DGEBA and other epoxy resins [7]. This is because DGEBA and epoxy group on other resin are directly connected on their ring, whereas alicyclic epoxy resins' epoxy groups are connected on aliphatic hydrocarbon or benzene nucleus. Alicyclic epoxy resins' curing products have high compressive and tensile strength. Moreover, the alicyclic epoxy resin could remain good mechanical properties at high temperature for long term. The molecular structure of the following epoxy resins are shown in Figure 2.7.

The epoxy resins before curing is a sticky liquid. It needs to be cured into a three dimensional cross linking network structure before being put into use. Such curing process is a reaction between the epoxy group and the curing agent (also called hardener). The reaction between epoxy groups and hardeners is able to form a three dimensional cross linking network structure and therefore the epoxy resin is able to cure into solid materials which are firm and infusible. Most of the epoxy resins, for example, bisphenol-A type epoxy resin, have strong temperature stabilities. The bisphenol-A type epoxy resin is able to remain unchanged even at 200 °C. However, different epoxy resins have different curing requirements. Some epoxy resins are able to cure under low temperature or room temperature, whereas others need to cure under high temperature. To some extent, the resulting curing products' properties are also being influenced by the curing agent. As the curing agent is able to influence epoxy resins properties significantly, it is also necessary to consider the curing agents used according to the epoxy resins properties and curing process requirements.

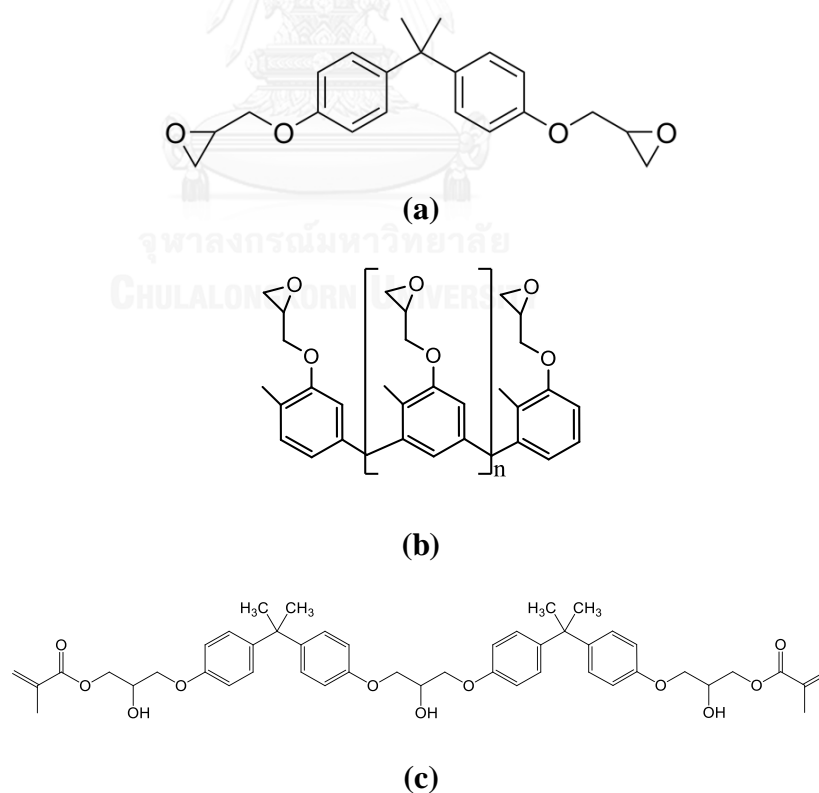


Figure 2.7 Molecular structures of (a) bisphenol-A type epoxy resin
(b) Novolac epoxy resins (c) glycidyl ester resins [6]

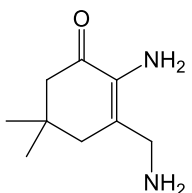
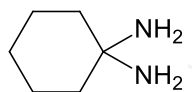
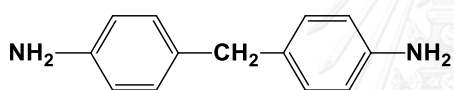
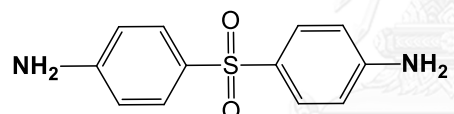
Amine curing agents

Amine is an important curing agent for epoxy resins and can be divided into three groups. First, aliphatic amine and derivatives, these are low-viscosity materials with high reactivity and fast cure at ambient temperatures. Aliphatic amines are used principally in civil engineering applications such as in patch repair systems, adhesives, floorings, high solid coatings and grouts. Some examples of aliphatic amine curing agents are primary aliphatic amines e.g. diethylenetriamine (DETA) and triethylenetetramine (TETA).

Second group includes cycloaliphatic and tertiary aliphatic amines. This group of curing agents is used at milder conditions than the aromatics amine but give elevated-temperature performance and chemical resistance of cured resins. They have found usage in adhesive and coating applications.

Lastly, aromatic amines such as 4,4'-diaminodiphenylsulfone (DDS), 4,4'-diamino diphenyl methane (DDM) and m-phenylenediamine (MPDA) are used to cure epoxy resins at high temperatures and at long cure times resulting from the rigid benzene ring in their structure. The aromatic amines are widely used in composite fabrication in both wet and dry lay-up application for filament winding, electrical, piping and tooling. Some examples of commercial curing agents are presented in Table 2.1.

Table 2.1 Commercial curing agents [7]

Formula	Name	Abbreviation
Aliphatic amines		
$\text{NH}_2\text{CH}_2\text{CH}_2\text{NHCH}_2\text{CH}_2\text{NH}_2$	Diethylenetriamine	DETA
$\text{NH}_2\text{CH}_2\text{CH}_2\text{NHCH}_2\text{CH}_2\text{NHCH}_2\text{CH}_2\text{NH}_2$	Triethylenetetramine	TETA
Cycloaliphatic amines		
	Isophoronediamine	IPDA
	1,2-Diaminocyclohexane	DACH
Aromatic amines		
	4,4'-Diaminodiphenylmethane	DDM
	4,4'-Diaminodiphenylsulfone	4,4'-DDS

2.3 Silica Surface Modification [8]

Among the numerous inorganic/organic hybrid materials, silica-polymer hybrid materials are one of the most commonly reported material. This may be attributed to their wide use and the ease of particle synthesis. Silica nanoparticles have been used in rubber products, colloidal products, paints, catalysis and plastic binders [9]. One of the important applications of silica is the use of it as a filler in polymer matrix for reinforcement. Silica nanoparticles have a noticeable reinforcing effect due to its high surface area which leads to a significant increase in the interfacial area in the polymer matrix. However, the hydroxyl group ($-OH$) on the silica surface absorbs moisture and increase polarity. This make silica nanoparticles tend to agglomerate, resulting in inferior compatibility and less stability between the polymer matrix and silica nanoparticle [10]. This problem could be resolved by surface modification of the silica nanoparticles.

Generally the surfaces of inorganic materials can be functionalized with polymer chains or organic compounds either chemically (through covalent bonding) or physically (by physisorption). Physisorption involves adsorption of polymers or organic compounds with sticky segments. The noncovalent adsorption makes the adsorption reversible, especially during processing. This make physisorption not a favored technique. Covalent grafting techniques are preferred to maximize a stable interfacial compatibility between the two phases. In the other hand, chemical treatment of the nanoparticle surface achieve better compatibility and dispersion of the filler in the polymer matrix. Chemical methods involve modification with modifying agents or by grafting polymers. The modifiers or coupling agents should have dual functional groups, one for surface binding and the other for initiating the designed chemical reactions. Therefore, silane coupling agents usually been used to treat the silica surface due to their unique bifunctional structure. The use of coupling agents is essential to obtain homogeneous mixtures between the organic and inorganic phases, by enhancing the interaction between the components at the interface level. Table 2.2. shows a number of typical silane coupling agents of the type $[R^1-Si(OR^2)_3]$, where R^1 is a functional group, such as aminopropyl or mercaptopropyl, and R^2 is a methyl or ethyl

group, which are commonly used in the preparation of hybrid silica-polymer materials for high performance coatings. The chemical properties of the silica surface are mainly determined by the various silanol and siloxane groups that are present on the external as well as the internal structure. The hydroxy groups on the surface of silica particles can be easily tailored with organic compounds or polymers as shown in Figure 2.8.

Therefore, chemical treatment of the nanoparticle surface is necessary to achieve better compatibility and dispersion of the filler in the polymer latex. This treatment lead to the bonding between the coupling agent and the silica surface. The replacement of hydroxyl group with coupling agent change the hydrophilic surface into a hydrophobic surface as shown in Figure 2.9

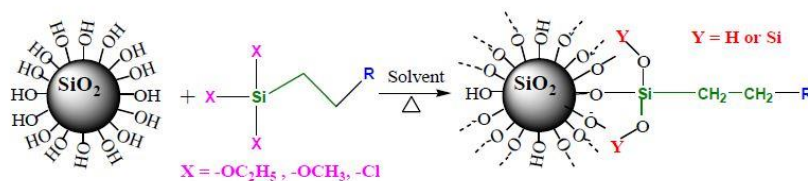


Figure 2.8 Surface modification of silica nanoparticles [10]

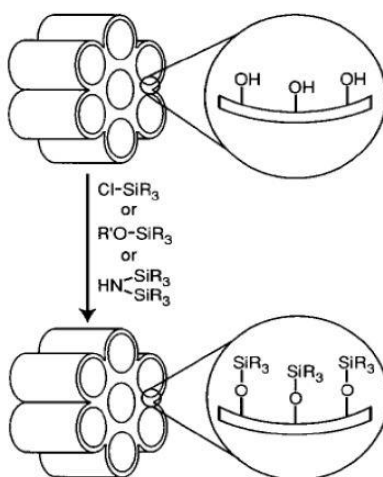
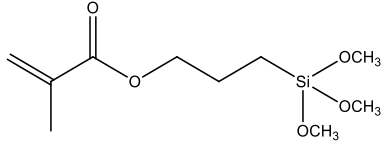
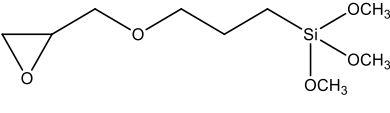
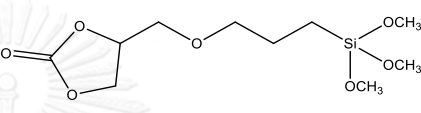
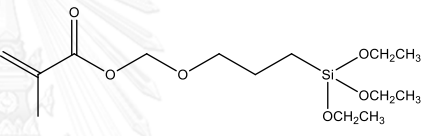
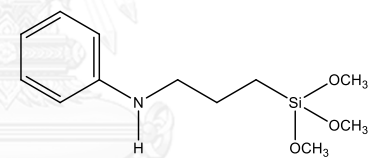
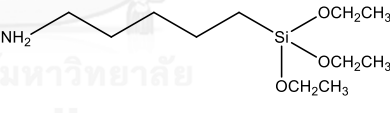


Figure 2.9 Functionalization of silica nanoparticles [10]

Table 2.2 Typical silane coupling agents used in the preparation of hybrid silica-polymer materials [11-16].

Abbreviation	Name	Chemical Structure	References
MPS	3-Methacryloxypropyl trimethoxysilane		[11]
GPTMS	Glycidoxypropyltrimethoxysilane		[12]
CPS	4-((3-(Trimethoxysilyl)propoxy)methyl)-1,3-dioxolan-2-one		[13]
MPTES	3-Methacryloxypropyl triethoxysilane		[14]
PATMS	<i>N</i> -[3-(trimethoxysilyl)propyl]aniline		[15]
APTES	3-Aminopropyl triethoxysilane		[16]

2.4 Epoxy/Silica Nanocomposite [17]

Epoxy resins, as organic matrix, have excellent heat, moisture, chemical resistance and good adhesion to many substrates. They are mostly applied in the field of coatings, adhesives, laminates, casting, composite and encapsulation of semiconductor devices [18]. However, due to their low mechanical properties, the epoxy resins cannot meet all the requirements of applications, especially for the applications of coating which required proper mechanical properties and chemical resistance to be used in various field. Organic/inorganic hybrid materials are frequently utilize in order to overcome the lack of mechanical properties in epoxy resin. They combine the advantages of the inorganic material (e.g., rigidity, thermal stability) and the organic polymer (e.g., flexibility, dielectric, ductility, and processability). Moreover, they usually contain special properties of nanofillers leading to materials with improved properties.

Hybrid nanocomposite materials can be prepared by two separated methods, either the addition of preformed inorganic particles, i.e. spherical silica nanoparticles, or the *in situ* growth of siloxane clusters. Both *in situ* siloxane clusters and silica particles are commonly used for the reinforcement of epoxy matrix to lower shrinkage on curing, decrease coefficient of thermal expansion, improve thermal conductivity and barrier properties, and to meet mechanical requirements. The intrinsic properties of each filler component, the shape of fillers, the nature of the interface, and so forth largely affect the properties of hybrid materials [19]. Therefore, for excellent properties, strong interfaces between components are needed. Another important factor of fillers for affecting composite properties are their content and size. To enhance the hybrid nanocomposite properties, smaller size and larger amount of fillers are required. It has been already reported that the increase of specific surface and fillers contents enhance the mechanical and impact properties of composite [17]. However, when the size of fillers becomes smaller and the fillers content higher, the viscosity of composite resin will be too high to process. In that case, the interfacial strength will be more important factor due to their increasing surface area of fillers. One of the most promising solutions

for enhancing processability at high filler-loading system is suggested to be the surface modification of fillers [8].

Ochi et al. [20] studied the preparation of epoxy/silica nanocomposite materials by using Biphenol-A type epoxy resin and alkoxy silane as organic and inorganic sources, respectively. The composite was synthesized via sol-gel reaction of the alkoxy silanes during the progress of epoxy curing. By following this route of hybrid preparation, a contemporaneous growth of the two networks are allowed. The epoxy-based hybrid materials exhibited good thermal stability and mechanical properties in the high temperature region even with low silica content (<10 wt%). Moreover, the use of GPTMS coupling agent in the epoxy grafted silicone oligomer hybrid samples showed to enhance the morphological control. TEM images showed fine silica-rich domains of about 5 nm in diameter uniformly dispersed in the cured epoxy matrix. Additionally, the storage modulus in the rubbery region and the peak area of the $\tan \delta$ curve at the glass transition region increased and decreased, respectively, with the hybridization of organic network. Therefore, the mobility of the epoxy network chains should be considerably suppressed by the hybridization with siloxane structures.

Mascia et al. [21] studied the influence of the geometrical configurations of the inorganic phase within an organic matrix on the physical properties of hybrids materials. They aimed to build up a chemical bond between organic/inorganic hybrids. 3-Glycidoxypropyltrimethoxysilane (GPTMS) and aminosilanes were used as coupling agents. In particular, GPTMS was used to functionalize the inorganic silica particles obtained by TEOS during the sol-gel process, whereas several kinds of aminosilanes such as Bis-(γ -propyltrimethoxysilane)amine A1170 and Mercapto γ -propyltrimethoxysilane MPTMS were reacted with Diglycidylether of Bisphenol A (DGEBA). They found that the surface functionalization on the silica inorganic filler, both GPTMS and aminosilanes, enhanced the dispersion of silica inorganic filler in the epoxy matrix. The presence of organic coupling agents on silica nanoparticle surface increase the hydrophobicity properties which make silica form less cluster and show good dispersion as shown in Figure 2.10

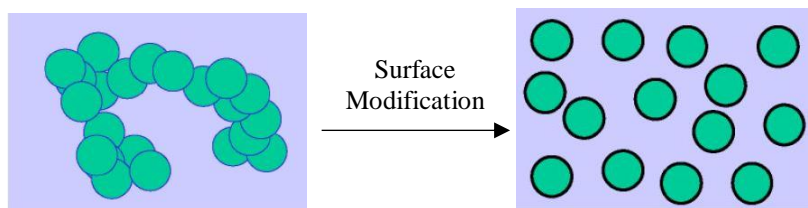


Figure 2.10 Scheme of surface modification for nano-size filler [20].

Moreover, Matejka et al. [22] described the formation, structure and properties of DGEBA-Jeffamine D2000-TEOS hybrid materials. The effect of both the catalyst and the synthesis procedure used for the preparation of hybrids materials was studied. The hybrid material was prepared by using two methods, the one-step polymerization, in which all the organic and inorganic component were obliged to react altogether, and the two step polymerization of silica, which consisted of prehydrolysis of TEOS in acid medium in the first stage, followed by the build-up of a network in the presence of the amine hardener. The morphology of the network synthesized by the one-step base-catalyzed simultaneous polymerization was the most heterogeneous one. Large siloxane aggregates with a size of about 100-300 nm was detected. It composed of smaller clusters of 20-70 nm in diameter. Whereas the two step acid-base polymerization showed smaller siloxane clusters and fine dispersion of inorganic domains. Regardless the preparation procedure, all the hybrid composite samples showed improvement in their dynamic mechanical behavior compared to the neat epoxy network. Furthermore, in the dynamic mechanical analysis (DMA) curves of the two-step polymerization hybrids, a new relaxation peak at higher temperature could be observed. This provided evidence of such a phase separation in the epoxy-silica hybrids.

2.5 Characterization of Epoxy/Silica Nanocomposite

There are many methods to characterize the anticorrosion properties of nanocomposite. Basically, corrosive agents usually come in contact with coating film in liquid form. Therefore, the easiest way is to investigate the contact angle of water on the nanocomposite surface (wettability). However, wettability result alone could not conclude the anticorrosion performances. Therefore, electrochemical behavior was performed to confirm the wettability result and to identify the corrosion rate of the nanocomposite.

Wettability

Wettability is used to identify the ability of a fluid to spread or adhere on a surface. The degree of wetting in a matrix-fluid system is dependent on the interfacial tension (IFT), σ , between the fluid and the solid surface. It can be measured by the contact angle, θ , which occurs at the fluid-fluid interface on the solid. For $\theta < 90^\circ$ the fluid is defined as wetting phase and for $\theta > 90^\circ$ the fluid is non-wetting, as illustrated in Figure 2.11. Angles equal to 90° indicates neutral or intermediate wetting and for $\theta \sim 180^\circ$ the phase is totally wetting.

Tafel Plots

This electrochemical measurement technique is used to measure the corrosion current (I_{corr}) so that the corrosion rate can be calculated. A Tafel plot can yield I_{corr} directly or it can yield the Tafel constants, β_A and β_C as shown in Figure 2.12. The Tafel constants can then be used with the polarization resistance (R_p) value to calculate I_{corr} .

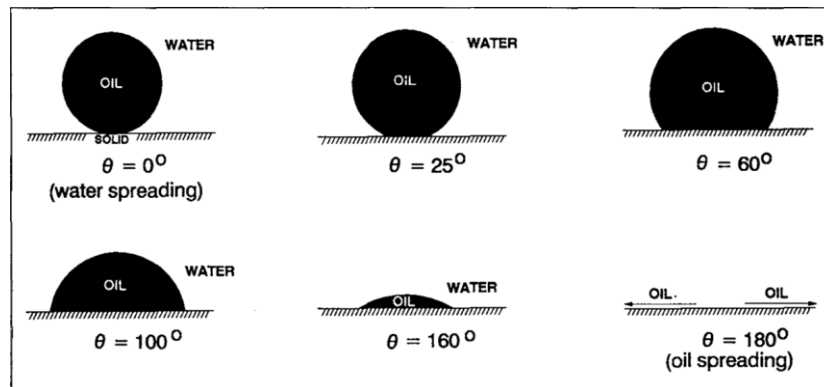


Figure 2.11 Wettability illustrated by examples of contact angles and spreading [22].

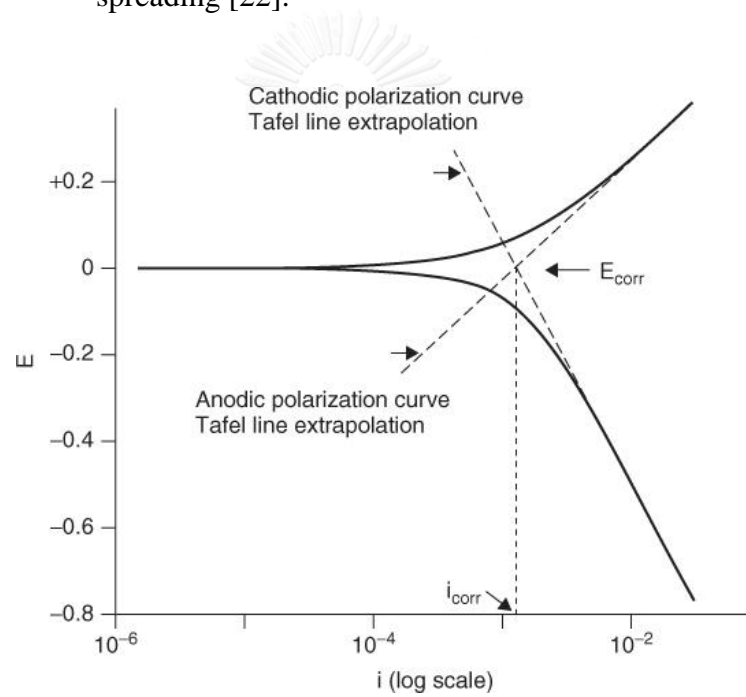


Figure 2.12 Combined anodic and cathodic Tafel plots [23].

2.6 Corrosion [23]

Corrosion is the deterioration of materials by chemical interaction with their environment. The term corrosion is sometimes also applied to the degradation of plastics, concrete and wood, but generally refers to metals. The most widely used metal is iron (usually as steel). Most environments are corrosive to a greater or lesser degree. Examples are air and moisture; fresh, distilled, or salt water; rural, urban and industrial atmospheres; steam and other gases such as chlorine, ammonia, hydrogen sulfide, sulfur dioxide, and fuel gases; mineral acids such as hydrochloric, sulfuric and nitric; organic acids such as naphthenic, acetic, and formic; alkalis; soils; solvents such as alcohols and dry cleaning fluid and petroleum oils. The consequences of corrosion are many and varied and the effects of these on the safe, reliable and efficient operation of equipment or structures are often more serious than the simple loss of a mass of metal. Failures of various kinds and the need for expensive replacements may occur even though the amount of metal destroyed is quite small. Some of the major harmful effects of corrosion can be summarized as follows:

1. Reduction of metal thickness leading to loss of mechanical strength and structural failure or breakdown. When the metal is lost in localized zones so as to give a cracklike structure, very considerable weakening may result from quite a small amount of metal loss.
2. Hazards or injuries to people arising from structural failure or breakdown (e.g. bridges, cars, aircraft).
3. Loss of time in availability of profile-making industrial equipment.
4. Reduced value of goods due to deterioration of appearance.
5. Contamination of fluids in vessels and pipes (e.g. beer goes cloudy when small quantities of heavy metals are released by corrosion).
6. Perforation of vessels and pipes allowing escape of their contents and possible harm to the surroundings. For example a leaky domestic radiator can cause expensive damage to carpets and decorations, while corrosive sea water may enter the boilers of a power station if the condenser tubes perforate.

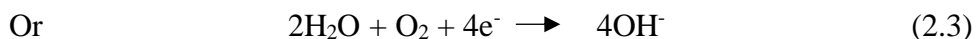
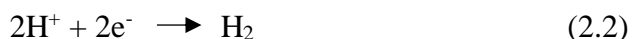
7. Loss of technically important surface properties of a metallic component. These could include frictional and bearing properties, ease of fluid flow over a pipe surface, electrical conductivity of contacts, surface reflectivity or heat transfer across a surface.

Nearly all metals, with the exception of gold and platinum, will be corroded in an oxidizing environment forming compounds such as oxides, hydroxides and sulfides. The degradation of metals by corrosion is a universal reaction, caused by the simple fact that the oxide of a metal has a much lower energy than the metal itself. Hence, there is a strong driving force for the oxidation of metals. Corrosion reactions are electrochemical in nature, at anodic sites on the surface, the iron goes into solution as ferrous ions, this constituting the anodic reaction. As iron atoms undergo oxidation to ions they release electrons whose negative charge would quickly build up in the metal and prevent further anodic reaction, or corrosion. Thus, this dissolution will only continue if the electrons released can pass to a site on the metal surface where a cathodic reaction is possible. At a cathodic site the electrons react with some reducible component of the electrolyte and are themselves removed from the metal. The rates of the anodic and cathodic reactions must be equivalent according to Faraday's Laws, being determined by the total flow of electrons from anodes to cathodes which is called the "corrosion current" (I_{corr}) [24]. Since the corrosion current must also flow through the electrolyte by ionic conduction, the conductivity of the electrolyte will influence the way in which corrosion cells operate. The corroding piece of metal is described as a "mixed electrode" since simultaneous anodic and cathodic reactions are proceeding on its surface as showed in Figure 2.13. The mixed electrode is a complete electrochemical cell on one metal surface. The most common and important electrochemical reactions in the corrosion of iron are as follows.

Anodic reaction (corrosion)



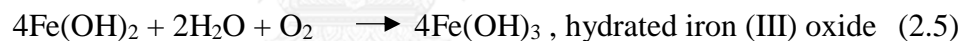
Cathodic reactions (simplified)



Reaction (2.2) is most common in acids and in the pH range 6.5 – 8.5 the most important reaction is oxygen reduction (2.3) In this latter case, corrosion is usually accompanied by the formation of solid corrosion debris from the reaction between the anodic and cathodic products.



Pure iron (II) hydroxide is white but the material initially produced by corrosion is normally a greenish colour due to partial oxidation in air.



Further hydration and oxidation reactions can occur and the reddish rust that eventually forms is a complex mixture whose exact constitution will depend on other trace elements which are present. Because the rust is precipitated as a result of secondary reactions, it is porous and absorbent and tends to act as a sort of harmful poultice which encourages further corrosion. For other metals or different environments, different types of anodic and cathodic reactions may occur. If solid corrosion products are produced directly on the surface as the first result of anodic oxidation, these may provide a highly protective surface film which retards further corrosion, the surface is then said to be “passive”. An example of such a process would be the production of an oxide film on iron in water, a reaction which is encouraged by oxidizing conditions or elevated temperatures.

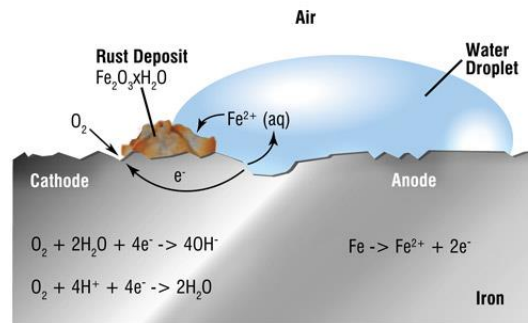


Figure 2.13 The formation of rust in iron via electrochemical reaction. [23]

2.6.1 Types of Corrosion

There are a number of different kinds of corrosion, depending on the types of materials involved and the nature of the surrounding media (Figure 2.14).

Galvanic corrosion occurs when dissimilar metals are put together in the same electrically conductive medium. The metal that is more oxidation resistant becomes the cathode, while the less resistant metal is the anode and undergoes rapid corrosion.

Concentration cell corrosion occurs when the conductive fluid that surrounds the metal is not homogeneous. Cathodes and anodes form because of differences in ionic concentration between different regions of the medium. The resulting corrosion is highly localized and often results in pitting.

Pitting is a type of corrosion that may be described as a condition intermediate between general corrosion and passivity (no corrosion). With pitting the corrosion takes the form of many small holes over the surface of the metal.

Stress corrosion cracking is caused by a combination of internal stresses that occur during processing and corrosion. In this case corrosion proceeds very rapidly at the spot where the stresses are concentrated and failure of the material may be very immediately.

Intergranular corrosion occurs at the grain boundaries of the metal due to the presence of impurities or stresses. Corrosion occurs on exposure of the metal's surface to a corrosive medium.

Uniform corrosion attacks the entire piece of metal. It can be caused by exposure to substances such as strong acid.



Figure 2.14 Types of corrosion: (a) Galvanic corrosion, (b) Concentration cell corrosion, (c) Pitting, (d) Stress corrosion cracking, (e) Intergranular corrosion and (f) Uniform corrosion attacks [24]

2.6.2 Corrosion Prevention [23]

By retarding either the anodic or cathodic reactions, the rate of corrosion can be reduced. This can be achieved in several ways:

Conditioning the metal

Coating the metal, in order to interpose a corrosion resistant coating between metal and environment, coatings such as paint forms a barrier between the metal and its environment.

Alloying the metal, to produce a more corrosion resistant alloy, e.g. stainless steel, in which ordinary steel is alloyed with chromium and nickel. Stainless steel is protected by an invisibly thin, naturally formed film of chromium sesquioxide Cr_2O_3 .

Conditioning the corrosive environment

Removal of Oxygen, by the removal of oxygen from water systems in the pH range 6.5-8.5, one of the components required for corrosion would be absent. The removal of oxygen could be achieved by the use of strong reducing agents e.g. sulfides. However, for open evaporative cooling systems, this approach to corrosion prevention is not practical since fresh oxygen from the atmosphere will have continual access.

Corrosion Inhibitors, A corrosion inhibitor is a chemical additive, which, when added to a corrosive aqueous environment, reduces the rate of metal wastage.

2.7 Self-Healing Materials [25]

Self-healing is defined as “the ability of a material to heal (recover/repair) damages automatically and autonomously, that is, without any external intervention” [26]. This definition does not specify to which extent and which properties of the material are restored/repared. In the broadest sense, self-healing materials can be distinguished as materials which are able to autonomously (partially) restore (some of) their properties in such a manner that they can serve longer as compared to similar materials without self-healing capabilities. If after rupture, at least one property of the material is restored at least partially without any external intervention, one can speak about self-healing capabilities of the material.

The main function of coatings is the protection of an underlying substrate against an environment-induced corrosion attack. Application of organic coatings is the most common and cost effective method of improving the corrosion protection and, thereby, the durability of metallic structures. A wide range of engineering structures, from cars to aircrafts, from chemical factories to household equipment, is effectively protected by coatings. The main role of an organic polymer coating in corrosion protection is to provide a dense barrier against corrosive species. Along with these barrier properties, resistance to a flow of charge, electronic and ionic, is also important since corrosion processes involve the transfer of charge. However, defects appear in organic protective coatings during exploitation of the coated structures opening a direct

access for corrosive agents to the metallic surface. The corrosion processes develop faster after disruption of the protective barrier. Therefore, an active “self-healing” of defects in coatings is necessary in order to provide long-term protection. In the case of corrosion protective coatings, the term self-healing can be interpreted in two different ways. From one perspective, only full recovery of the coatings functionality including mechanical and barrier properties of the coating is considered as “healing”. From another perspective, the main function of anticorrosion coatings is the protection of an underlying metallic substrate against an environment-induced corrosion attack. Thus, it is not obligatory to recuperate all the properties of the film in this case. The hindering of the corrosion activity in the defect by the coating itself employing any mechanisms can be already considered as self-healing, because the corrosion protective system recovers its main function, namely, the corrosion protection, after being damaged. The idea of a coating suitable for the reflow-healing of defects is a capsule-based self-healing approach. The repair of the coating is achieved through microencapsulated polymerizable agents incorporated into the coating matrix. If the coating is damaged, the microcapsules rupture, leaching the film forming components in the immediate vicinity of the damage (Figure 2.15). The fluid flows over exposed areas of the surface and fills any defects or cracks in the coating renewing the protective barrier.

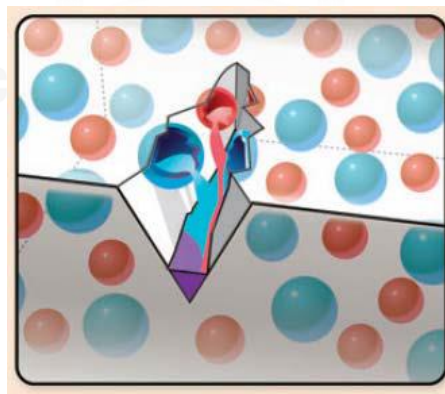


Figure 2.15 Illustration of the capsule-based sealing approach [26]

2.8 Literature Reviews

Huang et al. [27] studied advanced anticorrosive coatings prepared from electroactive epoxy–SiO₂ hybrid nanocomposite materials. A series of electroactive epoxy/amino-SiO₂ nanocomposite materials containing conjugated segments of electroactive amino-capped aniline trimer (ACAT) and nano-silica particles of ~50 nm in diameter were prepared. The amino-modified silica (AMS) particles of ~50 nm in diameter were synthesized by performing the conventional base-catalyzed sol–gel reactions of tetraethyl orthosilicate (TEOS) in the presence of (3-aminopropyl) trimethoxysilane (APTES) molecules. Subsequently, the AMS nanoparticles were blended into the epoxy ring-opening polymerization reactions between amino-terminated aniline trimer (ACAT)/T-403 and DGEBA, leading to the formation of electroactive epoxy resin–silica hybrid nanocomposite (EES). According to electrochemical measurement, EES exhibited a good anticorrosion property. The mechanism of anticorrosion property for EES could be attributed the synergistic effect of formation of passive metal oxide layers induced from redox catalytic capabilities of ACAT units, and gas barrier property induced from well-dispersed silica nanoparticles in its matrix. The synergistic effects make the EES coatings to reveal advanced corrosion protection efficiency as compared to that of non-electroactive epoxy (NEE) and electroactive epoxy (EE) and bare CRS electrodes based on the sequential electrochemical corrosion measurements in saline condition.

Ghanbari and Attar [28] studied the anticorrosion performance of epoxy nanocomposite coatings containing epoxy-silane treated nano-silica on mild steel substrate. The surface of nano-silica was treated with 3-Glycidoxypropyl-trimethoxysilane (GPTMS) in order to achieve proper dispersion of nanoparticles. Effect of treated nano-silica particles on the protective properties of epoxy coating was investigated. GPTMS coupling agent was employed to improve the dispersing of silica nanoparticles in epoxy coatings, and increasing possible chemical interactions of GPTMS functional groups on nanoparticle and polymeric matrix. EIS results revealed that 4–6 wt% incorporation of silica nanoparticles considerably enhanced the corrosion resistance of epoxy coating via increasing barrier properties, which made water and ion

species hard to transport and reduced the trend for substrate rusting and blistering of coating film. The incorporation of 4–6 wt% SiO₂ nanoparticles possessed the best corrosion performance.

Huang et al. [29] studied the synthesis of organic silane microcapsules for self-healing corrosion resistant polymer coatings. Hydrolysable organic silane, 1H,1H,2H,2H-perfluorooctyl triethoxysilane (POT), was carefully selected and microencapsulated as healing agent via *in situ* polymerization in an oil-in-water emulsion. The microcapsule size was adjustable via changing agitation rate for various coating systems. POT microcapsules were incorporated into epoxy resin and coated on a steel substrate to form a corrosion resistant organic coating. The self-healing coating displayed quite good corrosion protection ability to steel substrate via a fully self-healing mechanism. The self-healing behavior was realized under ambient condition, and it did not require any manual intervention such as heating or UV exposure, making it promising for the development of catalyst-free, one-part self-healing coatings, which is of considerable technical and commercial importance.

Cho and Kim [30] studied encapsulation of aliphatic amines into nanoparticles for self-healing corrosion protection of steel sheets. Polymeric nanocapsules loaded with six types of amine corrosion inhibitors were synthesized by multi-stage emulsion polymerization. Depending on the basicity and water solubility of amines, different amounts of releasable corrosion inhibitors were encapsulated into the polymer capsules. The nanocapsules were incorporated into the coating resin and were coated on cold-rolled steel sheets to investigate corrosion protection efficiencies. The amines with high water solubility were more efficient in both swelling and encapsulation than the amines with low water solubility. The encapsulation behaviors were also affected by the basicity of the amines. The amines that are strongly basic were more effectively encapsulated due to higher dissociation activity than the weak bases. Among six amines used in this study, 5-amino-1-pentanol, diethanolamine and triethanolamine exhibited self-healing anti-corrosion performance with recovering coating resistance. The corrosion resistance of the coating film gradually decreased and then increased via the self-healing protection of the amines

Hana Choi *et al.* [31] studied encapsulation of triethanolamine as organic corrosion inhibitor into nanoparticles and its active corrosion protection for steel sheets. Triethanolamine (TEA), a corrosion inhibitor for zinc and steel, was introduced into nano-sized particles as nanoreservoirs to increase longevity of inhibitive property and prevent degradation caused by direct addition of corrosion inhibitor into coating layer. TEA-incorporated nanoparticles with average particle size around 400–450 nm were successfully synthesized by sequential emulsion polymerization. In the corrosion tests, the encapsulated TEA decreased the corrosion rate of steel substrate owing to its adsorption on steel surface and the resistance of coating layer against corrosive environment was much higher and remained its resistance as immersion time increased when TEA was incorporated in coating layer in the encapsulated form. Based on the scanning vibrating electrode technique (SVET) result, anticorrosive ability of the encapsulated TEA seemed to improve due to the spontaneous passivation of exposed metal on the defected region of coated steel.

Kumar *et al.* [32] studied commercially synthesized urea-formaldehyde shell microcapsules containing various healing agents to determine their effectiveness when incorporated into paint primer coatings for steel surfaces. Under appropriate preparation conditions, several encapsulated compounds, including camphor and tung oil, exhibited a more than twofold reduction in damage as compared with microcapsule-free controls.

Brown *et al.* [33] studied *in situ* poly(urea-formaldehyde) microencapsulation of dicyclopentadiene. A process for the microencapsulation of dicyclopentadiene (DCPD) by *in situ* polymerization of urea-formaldehyde (UF) in an oil-in-water emulsion was developed to fulfill requirements for self-healing material applications. Microcapsules with average diameter in the range of 10-1000 μm were manufactured by varying the rate of agitation over the range 200-2000 rpm. As the agitation rate increased, the mean diameter decreased. Microcapsule shell thickness was 160-220 nm, providing excellent storage and release properties for self-healing applications. During the microencapsulation process UF nanoparticles formed and deposited on the microcapsule surface producing a rough surface morphology. Surface roughness enhanced mechanical adhesion of the microcapsules when embedded in a polymer and improved performance in self-healing applications.

Lange *et al.* [34] studied the influence of structure and chemical composition on oxygen permeability of crosslinked epoxy–amine coatings. The oxygen barrier properties of a series of coatings based on diglycidyl ethers of bisphenol and butanediol reacted with a wide range of amines in different stoichiometric ratios have been investigated. The oxygen permeability was analyzed with respect to the molecular structure in general and the concentration of polar functional groups in particular. The results showed that formulations based on aliphatic amines gave good barrier performance, that coatings prepared from aromatic and cyclo-aliphatic amines yielded intermediate barrier properties, and that polyether amine formulations produced very poor barriers. It was also observed that pendant methyl groups had a strong detrimental effect on barrier properties and that using an excess of amine monomer significantly improved the barrier performance.

Wetzel *et al.* [35] studied epoxy nanocomposite – fracture and toughening mechanisms. A comprehensive study was carried out on series of nanocomposite containing varying amounts of nanoparticles, either titanium dioxide (TiO_2) or aluminium oxide (Al_2O_3). The mechanical performance of the nanocomposite was then characterized by flexural testing, dynamic mechanical analysis (DMA), and furthermore, by fracture mechanics approaches (LEFM) and fatigue crack growth testing (FCP). It was found that the presence of nanoparticles in epoxy induced various fracture mechanisms, e.g. crack deflection, plastic deformation, and crack pinning. At the same time, nanoparticles could overcome the drawbacks of traditional tougheners (e.g. glass beads or rubber particles) by simultaneously improving stiffness, strength and toughness of epoxy, without sacrificing thermo-mechanical properties.

CHAPTER III

EXPERIMENTAL

3.1 Chemicals

- | | |
|---|-----------------|
| 1. Bisphenol A diglycidyl ether
(MW = 340.42 g·mol ⁻¹), AR grade | : Sigma-Aldrich |
| 2. Tetraethylenepentamine, AR grade | : Acros |
| 3. <i>p</i> -Phenylenediamine, AR grade | : Sigma-Aldrich |
| 4. Fumed nano-silica (Aerosil 200)
(Average particle size = 12 nm) | : Degussa |
| 5. (3-Aminopropyl)triethoxysilane, AR grade | : Sigma-Aldrich |
| 6. (3-Glycidyloxypropyl)trimethoxysilane
AR grade | : Sigma-Aldrich |
| 7. Ethanolamine, AR grade | : Sigma-Aldrich |
| 8. Diethanolamine, AR grade | : Sigma-Aldrich |
| 9. Sodium persulfate, AR grade | : Ajax Finechem |
| 10. Sodium dodecyl sulfate, AR grade | : QRëC |
| 11. Styrene, AR grade | : Sigma-Aldrich |
| 12. Methyl methacrylate, AR grade | : Sigma-Aldrich |
| 13. Butyl acrylate, AR grade | : Sigma-Aldrich |
| 14. Methacrylic acid, AR grade | : Sigma-Aldrich |
| 15. Xylene, AR grade | : QRëC |
| 16. Butanol, AR grade | : QRëC |
| 17. De-ionized water | |

3.2 Equipments

- | | |
|--|-------------------------------|
| 1. Fourier Transform Infrared Spectrophotometer
(FT-IR) | : Spectrum GX
Perkin Elmer |
|--|-------------------------------|

2. Thermal Gravimetric Analyzer (TGA)	: Perkin Elmer Pyris Diamond
3. Light microscope	: BX3M
4. Drop Shape Analyzer	: Model DSA25
5. Field Emission Scanning Electron Microscope and Energy Dispersive X-Ray Spectrometer (FESEM-EDS)	: JSM-7610F
6. Transmission Electron Microscope (TEM)	: TEM (2100)
7. Potentiostat/Galvanostat Instrument	: Autolab Type III
8. Salt Spray	: Q-FOG

3.3 Synthesis of Modified Silica Nanoparticles

3.3.1 APTES-modified Silica

The amino-modified silica (AMS) nanoparticles were prepared by two methods, conventional base-catalyzed sol-gel reactions and grafting reactions of APTES molecules. For conventional base-catalyzed sol-gel reactions of TEOS in the presence of APTES molecules, the AMS nanoparticles was synthesized by adding 4.17 g of TEOS, 0.48 mL of 1.0 N NaOH and 10.0 mL of dimethylacetamide (DMAc) in a 100 mL of three-neck round-bottom flask connected with a condenser. Then, the APTES 1.11 g was added into the TEOS gel solution with stirring for 30 min at room temperature. Nitrogen gas was bubbled into the flask throughout the reaction. Under the magnetic stirring, the solution was heated to 70 °C and maintained for 3 h. After cooling, the AMS particles were washed repeatedly with ethanol and separated from the aqueous mixture by centrifugal sedimentation, and dried under vacuum at room temperature for 48 h.

For the grafting reactions of APTES molecules onto silica nanoparticles, the AMS nanoparticles was prepared by adding 2 g of dried nano-silica dispersed in 60 mL of toluene then 1.7 g of amino-silane (APTES) was added. The slurry was stirred for 30 min at room temperature. Nitrogen gas was bubbled into the flask throughout the reaction. Under the magnetic stirring, the solution was heated to 70 °C and maintained

for 4 h. After cooling, the AMS particles were washed repeatedly with toluene to remove unreacted amino-silane and separated from the aqueous mixture by centrifugal sedimentation. The modified-silica was then dried at 80 °C in vacuum for 4 h before further used.

3.3.2 GPTES-modified Silica

The GPTMS-modified silica (GMS) nanoparticles were prepared via grafting reactions as shown in Figure 3.1. 2.0 g of dried nano-silica was dispersed in 50 mL ethanol and stirred for 1 h in ambient temperature. In the next step, 12 mL of GPTMS and 3.8 mL of deionized water were gradually added to the slurry and stirred for further 2 h. In order to have a maximum efficiency of silane hydrolysis, pH value in this step was adjusted to 2 using 1.0 M HCl. It should be noted that the reaction was performed at hydrolysis ratio of 3 (the ratio of water to silane). The mixture was refluxed for 48 h. After reflux, mixture was centrifuged (4000 rpm) and the residue was washed with ethanol and deionized water until neutral. The remained precipitate was dried in vacuum oven at 60 °C for 4 h.

3.4 Synthesis of Self-Healing Microcapsules

3.4.1 Synthesis of Perfluorooctyltriethoxysilane (POT) Loaded Microcapsules

The preparation of microcapsules was based on an *in situ* polymerization reaction in an oil-in-water emulsion system. 50 mL of deionized water and 12.5 mL of 2.5 wt% aqueous solution of ethylene maleic anhydride copolymer were mixed in a 500 mL beaker. The beaker was suspended in a temperature-controlled water bath on a hot plate with an external temperature probe. The solution was stirred at 400 rpm in ambient temperature. Under stirring, 1.25 g urea, 0.125 g ammonium chloride and 0.125 g resorcinol were dissolved in the solution. The pH value of the solution was raised from

about 2.6 to 3.5 by drop-wise addition of 1 M NaOH. 10 g POT and toluene were then slowly added into the above aqueous solution to generate emulsion, followed by the addition of 3.17 g of 37 wt.% aqueous solution of formaldehyde. The emulsion was covered and heated to 55 °C. After 4 h of continuous reaction, the microcapsules were collected for air-drying at room temperature for 48 h before further analysis.

3.4.2 Synthesis of Amine Loaded Microcapsules

Nano-sized polymeric capsules as reservoirs for carrying amine as a corrosion inhibitor were fabricated by sequential emulsion polymerization. The core latex was obtained from emulsion polymerization of methyl methacrylate (MMA), butyl acrylate (BA) and methacrylic acid (MA) with the ratio of 63:9:28 w/w as main components. Potassium persulfate was used as a free radical initiator and sodium dodecyl sulfate was used as an anionic emulsifier for emulsion polymerization. The polymerization process was carried out under nitrogen atmosphere, and deionized water (DI water) was used throughout all of the experimental processes. After 6 h of reaction, the core latex was formed. Then the core latex particles were dispersed in DI water at 80 °C with the presence of sodium persulfate to initiate radical reaction within 5 min. methyl methacrylate, butyl acrylate and methacrylic acid with the ratio of 90:7:3 w/w was added to create first shell layer with intermediate hydrophilicity on the hydrophilic core latex particles. This intermediate layer was employed for better encapsulation of hydrophobic polymer shell on the hydrophilic core polymer. After holding at 80 °C for 1 h, a stable monomer pre-emulsion of styrene was added into the reactor at the rate of 2.27 g/min. Once the formation of the outermost shell (polystyrene) is completed, the penetration of amine into the core through the shell will be difficult due to the rigidity of polystyrene shell. Therefore, amine was simultaneously fed with styrene pre-emulsion mixture for the first 15 min to maximize the encapsulation efficiency.

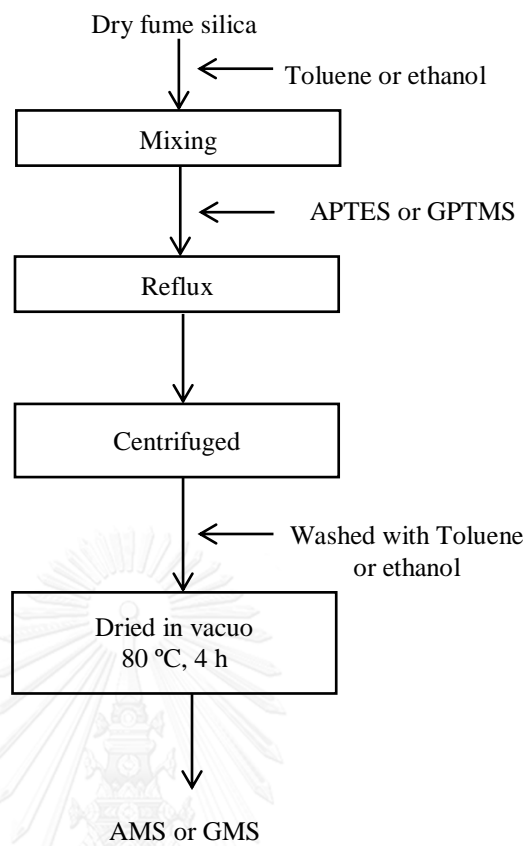


Figure 3.1 The schematic diagram of AMS and GMS synthesis

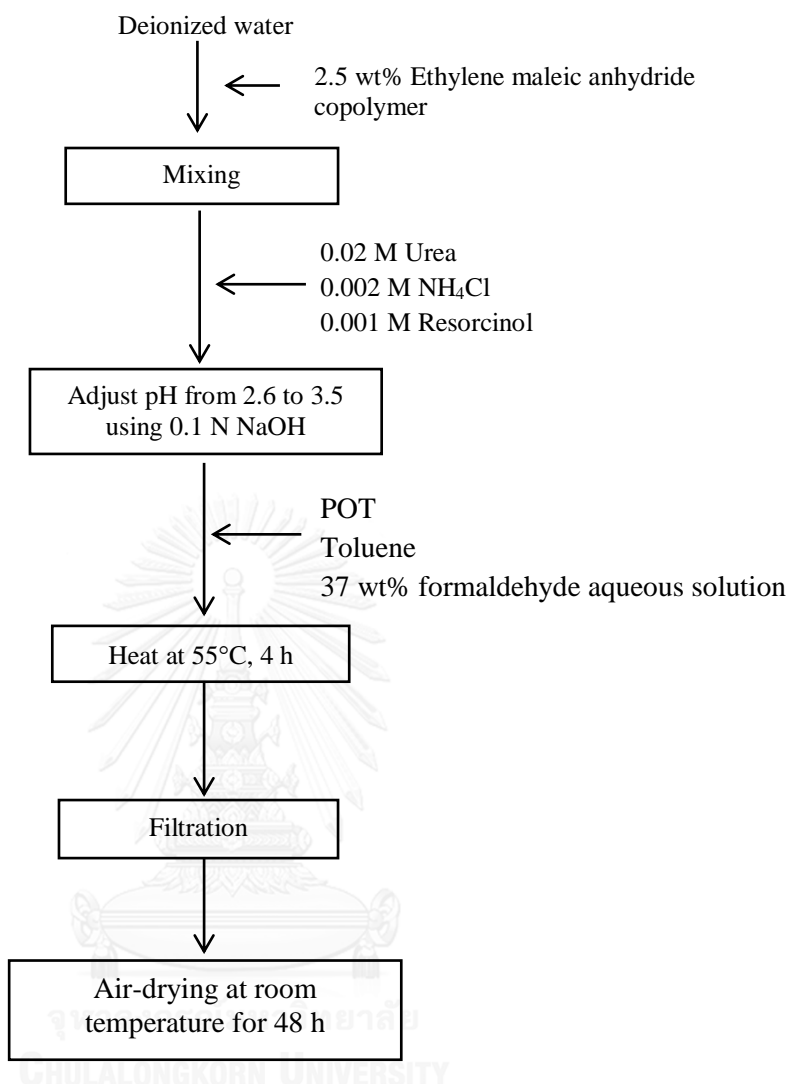


Figure 3.2 The preparation of perfluorooctyl triethoxysilane encapsulated in polymeric microcapsules

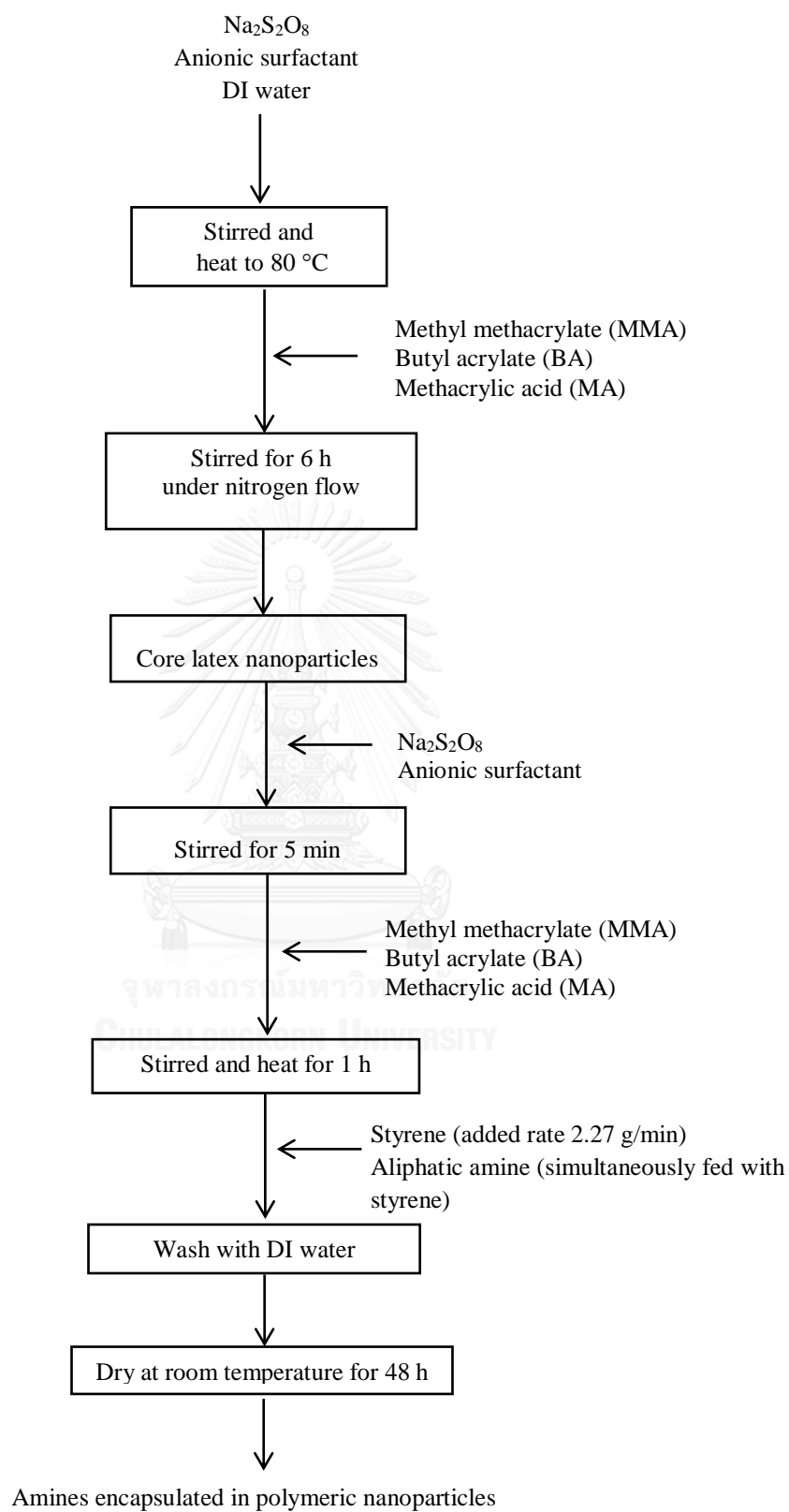


Figure 3.3 The preparation of amines loaded microcapsules

3.5 Coating of Epoxy Nanocomposite on Steel Samples

Diglycidyl ether of bisphenol-A was dissolved in xylene/butanol mixture (7:3). The nano-silica was gradually added to the epoxy polymer and stirred for 1 h at $30\pm 2^\circ\text{C}$. Then, curing agent (TEPA /*p*-PDA) was added to the mixture and stirred for 5-10 min before coating. During the mixing steps, neat epoxy, untreated silica, modified silica nanoparticles (1-5 wt%) and self-healing microcapsules (10 wt%) incorporated in the epoxy-hardener film were prepared. In order to make a suitable coating properties, an appropriate concentration of epoxy polymer and the curing agents were evaluated. The stoichiometric ratio of the resin to the hardener was adjusted to 10:1 in order to obtain an appropriate efficiency of the curing reaction. The prepared nanocomposite coatings were applied on the microscope slide with $25\text{ mm} \times 75\text{ mm}$ in dimensions and cold-rolled steel (CRS) coupons with $2\text{ cm} \times 5\text{ cm} \times 0.1\text{ cm}$ and $1\text{ cm} \times 1\text{ cm} \times 0.1\text{ cm}$ in dimensions. In order to remove any contaminants on the surface, the CRS coupons were mechanically polished using 150 and 400 grade emery papers followed by rinsing with distilled water and acetone before further coating. The coating was deposited by high-pressure air spray system (Figure 3.4(a) and (b)). The film was then allowed to dry in an oven at 60°C for 1 h. The effect of modified nano-silica, self-healing agents and type of hardener were studied. The thickness was measured using electronic outside micrometer. The measurement was taken from three different points distributed over the sample, and the reported values were averaged of three measurements.

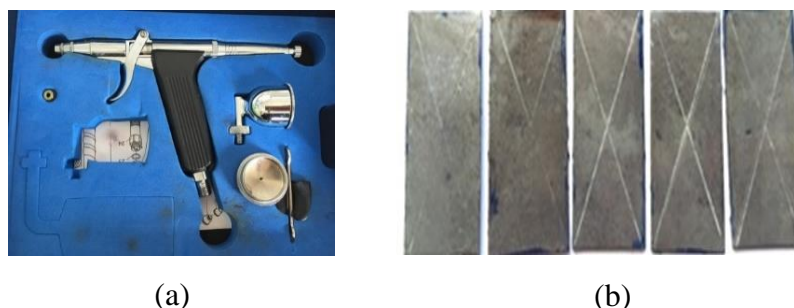


Figure 3.4 (a) Spray gun and (b) Steel coupons coated by spray method

3.6 Characterization Methods

3.6.1 Fourier Transform Infrared (FT-IR) Spectroscopy

Structures of epoxy/modified silica/self-healing nanocomposite were characterized using a Spectrum GX Perkin Elmer (USA) in the range of 400-4000 cm^{-1} with 32 scans. The samples were prepared by dispersion in potassium bromide (KBr) and compressed into a pellets.

3.6.2 Study of Dispersion of Silica

Optical microscope (Olympus BX 50, USA) was used to evaluate the dispersion of nano-silica in the epoxy polymer. The coated nanocomposite on the microscopoe slide was placed under optical microscope. The pictures were taken at the magnification of 40X and 200X.

3.6.3 Contact angle Measurement

The contact angle of hybrid nanocomposite coated on cold-rolled steel were evaluated using Drop Shape Analyzer model DSA25 (Germany). The sample surface was cleaned by ethanol and deionized water and then dried the surface. After the sample dried, it was fixed on the sample holder and adjusted horizontally. Then, a sessile drop of deionized water with a volume of 4 μL (less than 10 μL to satisfy the spherical assumption) was deposited carefully on the surface through a micro-syringe and its side view images were recorded by the CCD camera after around 1 min when the drop was formed. The sample was dried with tissue paper, and every repeated test was performed after more than 5 min.

3.6.4 Morphological Study

Scanning electron microscope (SEM, JEOL Model JSM-5410 LV, USA) was used to investigate the morphology of epoxy/modified silica/self-healing nanocomposite coated on cold-rolled steel. The completely dried samples were placed on SEM stubs and then coated with gold. The silica nanoparticle morphology was characterized using transmission electron microscope (TEM, JEOL JEM-2100, USA) at the acceleration voltage of 80 kV. The dilute nanoparticles were deposited on copper grid and kept in desiccator for 24 h before further analysis.

3.6.5 Cyclic Voltammetry

The electrochemical behavior of the epoxy/modified silica/self-healing nanocomposite was investigated by cyclic voltammetry (autolab type III/FRA2, USA). Epoxy/modified silica/self-healing nanocomposite was coated on carbon fiber cloth and used as working electrode in 1 M H₂SO₄ aqueous solution. The electrochemical behavior was studied at the potential range of -1V to +1V and scan rate of 50 mV/S. A Pt counter electrode and an Ag/AgCl reference electrode were used throughout of the studies.

Program : GPES

Method : cyclic voltammetry : normal

Parameter of potentials

Number of scans : 10

Begin potential (V) : 1

First vertex potential (V) : -1.0

Second vertex potential (V) : +1.0

Step potential (V) : 0.035

Scan rated (V/s) : 0.05

Surface area (cm²) : 1

3.6.6 Corrosion Study

The electrochemical Tafel slope analysis was used to evaluate the anticorrosive performance of epoxy/modified silica/self-healing nanocomposite coating on cold-rolled steel samples. Tafel plots for coated epoxy/modified silica/self-healing nanocomposite samples were recorded by sweeping the potential in the range of -1V to +1V against Ag/AgCl reference electrode in 1 M H₂SO₄ electrolyte as shown in Figure 3.5.

Program : GPES

Method : linear sweep voltammetry (staircase) : normal

Parameter of corrosion rate

Edit proceduced – Page 1

- Begin potential (V) : +1.0

- End potential (V) : -1.0

- Step potential (V) : 0.001

- Scan rated (V/s) : 0.001

- Surface area (cm²) : 1

Edit proceduced – Page 2

- Define (vertex) potential OCP : active

- Time to with for OCP : -1.0

- Tafel plot : active



Figure 3.5 The electrochemical Tafel slope analysis apparatus

The corrosion current (I_{corr}) was determined through superimposing straight line along the linear portion of the cathodic or anodic curve and extrapolating it through E_{corr} . The corrosion rate (R_{corr} , in millimeter per year, mm/year) was calculated from equation 3.1. Where E.W. is the equivalent weight (in g/eq.) of the CRS, A is the area (cm^2) of the coated CRS, and d is the density (g/cm^3) of the CRS.

$$R_{\text{corr}} = \frac{0.33 \times I_{\text{corr}} (\text{E.W.})}{A \times d} \quad (3.1)$$

The corrosion resistance of coated steel samples was measured according to the standard testing method ASTM B117 using salt spray tester. Salt spray test was an accelerated corrosion test that produces a corrosive attack to the coated samples in order to predict its suitability in use as a protective finish. The appearance of corrosion products was evaluated after a period of time. The apparatus for testing consists of a closed testing chamber, where a corrosive environment of dense saline fog was produced. The samples exposed in the chamber were subjected to severely corrosive conditions, and were tested continuously for the duration 96 h with 5 wt% NaCl solution. The period in testing without showing signs of corrosion increased with increasing the corrosion resistance of the coating.

CHAPTER IV

RESULTS AND DISCUSSION

Epoxy/modified silica/self-healing hybrid nanocomposite was successfully prepared. 3-Glycidoxypropyl-trimethoxysilane (GPTMS) and 3-aminopropyl-trimethoxysilane (APTES) were used to modify silica nanoparticles surface via grafting reaction in order to accomplish proper dispersion of nanoparticles in polymer matrix. Perfluorooctyl triethoxysilane (POT), ethanolamine (ETA) and diethanolamine (DEA) were encapsulated in polymer shell by *in situ* polymerization in an oil-in-water emulsion system as self-healing agents. The surface modification of nanoparticles and the presence of self-healing agents were characterized using Fourier transform infrared spectroscopy (FTIR). Optical microscope (OM) was used to observe the microstructure and dispersion of nanoparticles. The surface morphology of nanocomposite was observed by scanning electron microscopy (SEM). Anticorrosion performance of the coated CRS specimens was investigated by salt spray test, Tafel plot and cyclic voltammetry (CV).

4.1 Synthesis of Modified Silica Nanoparticles via Sol-gel Reaction

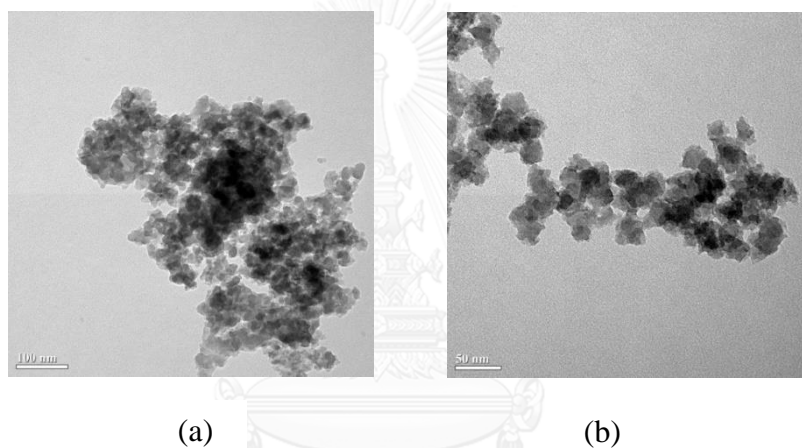
Amino-modified silica (AMS) were synthesized from base-catalysed sol-gel reaction of tetraethyl orthosilicate (TEOS) in the presence of APTES and NaOH as a catalyst. Figure 4.1 shows the morphology of synthesized silica nanoparticles observed by TEM. The shape of silica particles did not maintain the typical spherical shape. This could be explained by *in situ* modification in the synthetic process of silica particles. The random reaction between APTES and hydroxyl groups on silica surface occurred and greatly increased the irregular degree of the silica particles shape. The effect of TEOS:APTES molar ratio (4:0, 4:0.5, 4:1, 4:1.5 and 4:2) on number of amines functionalized on silica was investigated. The amount of amine grafted on silica particle was determined by direct titration method, based on Höfen et al., 2011 [36], and thermogravimetric analysis (TGA).

For direct titration method, an excess of sodium chloride was added to the particle suspension to provide a large excess of chloride ions that replaced quantitatively with the hydroxide ions, the counter ions of the ammonium groups, form NaOH at the ratio of 1:1 to the amino. The amount of NaOH was determined by titration with 0.1 M HCl. The results showed that increasing the amount of amine ratio of TEOS: APTES, from 4:0 to 4:2, the amount of the amino groups attached to the silica nanoparticles increased. However, the reference titration method of Hofen et al., studied on amino-modified silica particles via post grafting synthesis which amino groups were grafted to the silanol group on the silica particles. This indicated that the amino groups only attached to the external surface of the silica particle. Unlike this research, silica nanoparticles were synthesized by co-condensation, which amino groups were added during the synthesis, allowed amino groups to attach not only the external surface but also internal surface of the mesopore. Therefore, the amino groups obtained by titration method may not be correct due to the amino groups in the mesopore were not included.

The thermogravimetric analysis was also used to determine the amount of water and animosilane grafted on silica particle via dehydration and dehydroxylation reaction of silica particles. From Figure 4.2 (b), weight loss curve near 100 °C represent the loss of water in silica particle, and the second weight loss curve in the range of 260-800 °C indicated the decomposition of organic substance (APTES) on the silica particle. The amount of amine groups loaded obtained from both method is presented in Table 4.1

Table 4.1 The amount of amine groups obtained by direct titration and TGA

TEOS:APTES	Amount of APTES (% as TEOS)	Volume of 0.1M HCl (ml)	The amount of amine loading (%)	
			Direct titration	TGA
4:0	12.5	1.6	1.77	11.41
4:0.5	25	4	4.42	14.65
4:1	37.5	6.8	7.50	18.62
4:2	50	8	8.76	19.40

**Fig. 4.1** TEM images of amino-modified silica synthesized via sol-gel reaction (a) 180,000X and (b) 200,000X

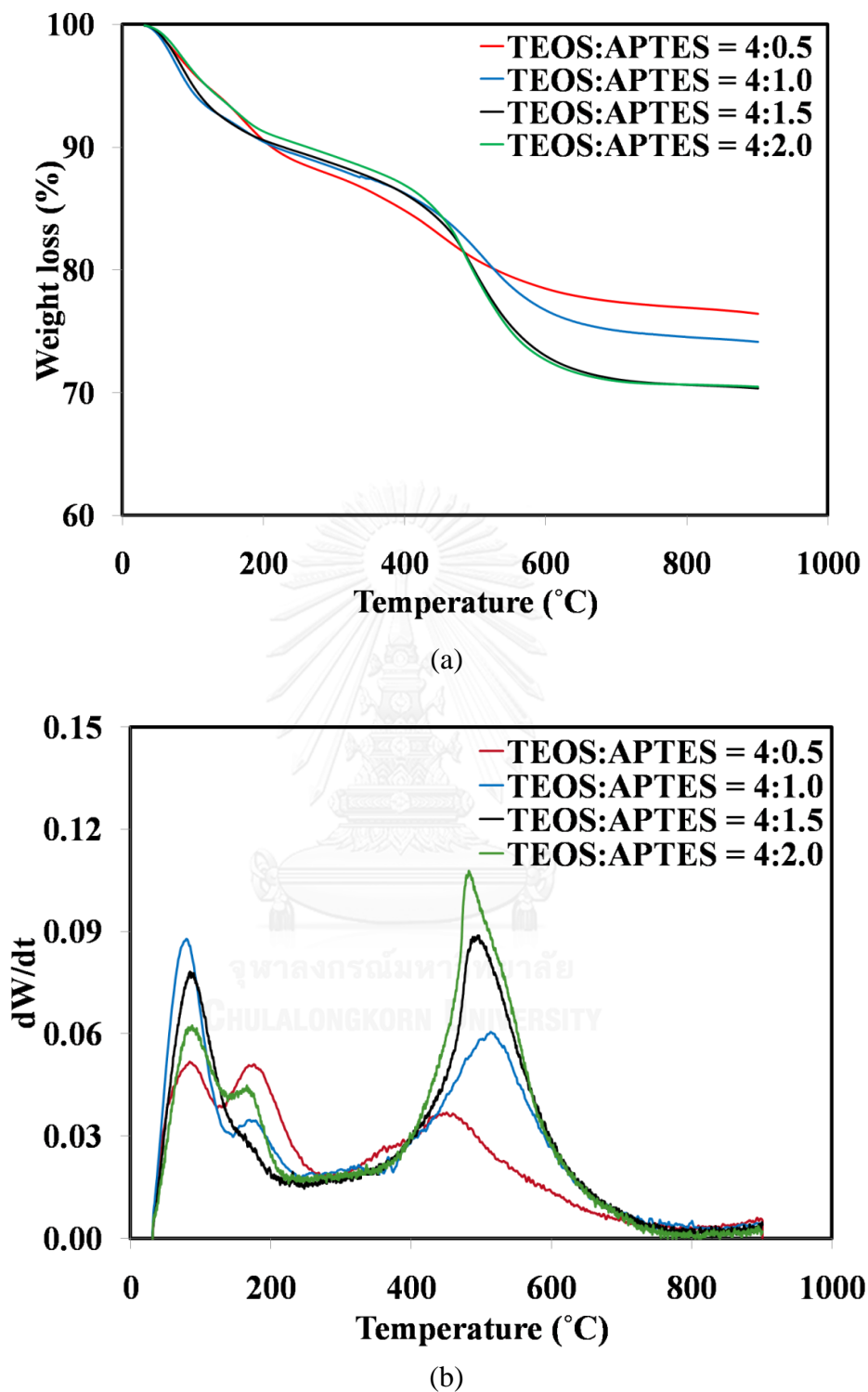


Figure 4.2 (a) TGA and (b) DTG curve of amino-modified silica nanoparticle with various APTES loading

4.2 Modification of Silica Nanoparticles

Silane coupling agents, APTES and GPTMS, were used to modify silica nanoparticle surface via grafting reaction to enhance the hydrophobicity properties. Fume silica with the average particle size of 12 nm was used as a precursor. Figure 4.3 shows TEM images of both APTES and GPTMS modified silica nanoparticles. After modification, the shape of silica nanoparticles remain a spherical shape with the average particles size increased to 20-25 nm in both AMS and GMS. The particle size of modified silica nanoparticles was confirmed by dynamic light scattering (DLS) as shown in Figure 4.4. The average particle size (\bar{D}_n) and particle size distribution (PSD) of modified silica nanoparticles are presented in Tables 4.1. It can be seen that the \bar{D}_n and PSD of AMS were 24.66 and 8.2 nm, respectively and % conversion was 68.1%. The \bar{D}_n and PSD of GMS were 23.48 and 9.1 nm, respectively and % conversion was 81.6%

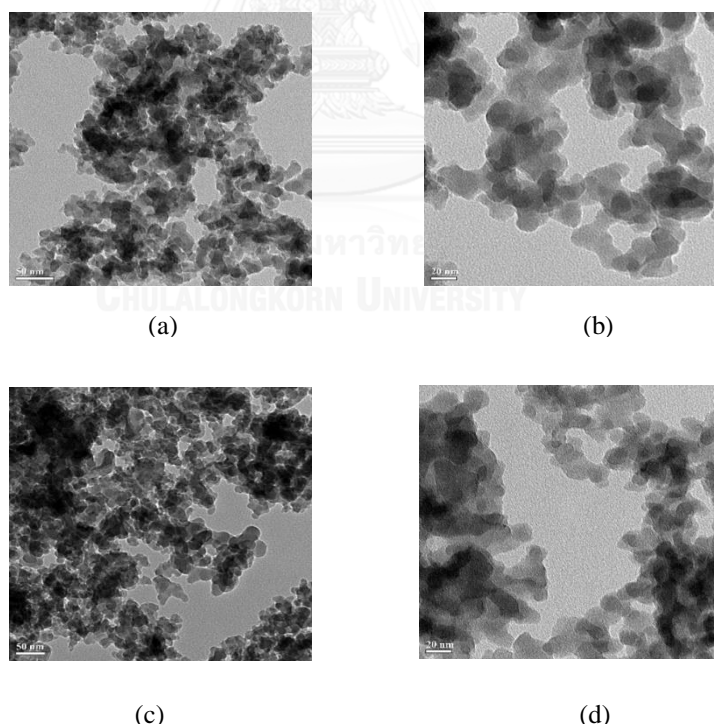


Figure 4.3 TEM images of APTES-modified silica nanoparticles at (a) 180,000X (b) 220,000X and GPTMS-modified silica nanoparticles at (c) 180,000X (d) 220,000X

Table 4.1 Amount on silica conversion, solid content, average particle size (\bar{D}_n) and particles size distribution (PSD) of modified silica nanoparticles

Sample	Conversion (%)	Solid Content (%)	\bar{D}_n (nm)	PSD (nm)
AMS	68.1	4.5	24.66	8.2
GMS	81.6	4.8	23.48	9.1

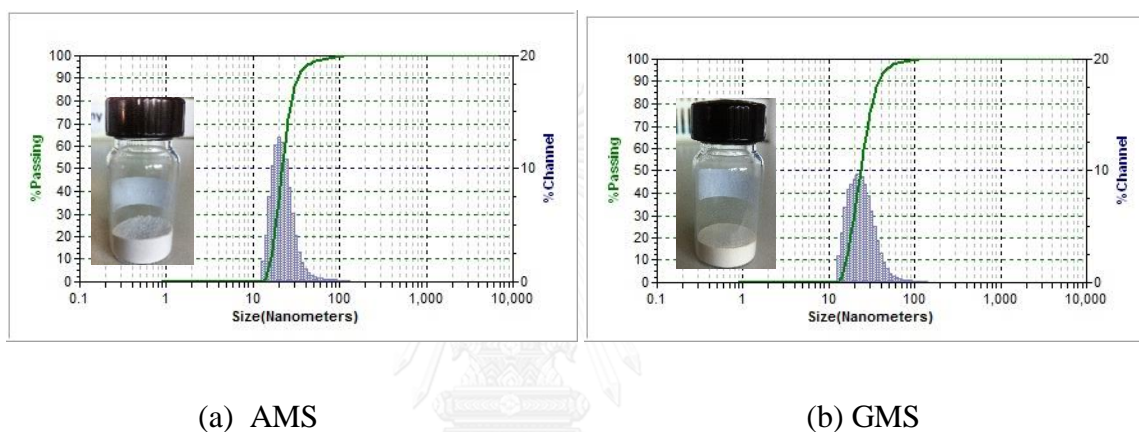


Figure 4.4 Particle size distribution of (a) AMS and (b) GMS

4.3 Synthesis of Self-Healing Microcapsules

4.3.1 Synthesis of POT Loaded Microcapsules

Poly(urea-formaldehyde) (PUF) microcapsules containing perfluorooctyl triethoxysilane (POT) as core materials were synthesized via *in situ* polymerization in an oil-in-water emulsion following an established method [29]. TEM image in Figure 4.5 shows that the resultant PUF microcapsules with POT, have a rough outer surface. For a microcapsule-based self-healing system, the diameter of embedded capsules greatly influenced the healing performance. The average diameter of microcapsules was 200 nm. It is found that the increase in agitation rate would result in smaller

microcapsules. The main reason for such a relation is that at higher agitation rate, finer oil droplets would form in the emulsion system due to stronger shear force. In the synthesis, the PUF membrane shell wall was formed surrounding the oil droplets. Therefore, the final microcapsules would accordingly be smaller at higher agitation rate. The particle size of POT loaded microcapsule was characterized by dynamic light scattering (DLS). The average particle size (\bar{D}_n) and particle size distribution (PSD) were 210 and 61.3 nm, respectively.

4.3.2 Synthesis of Amine Loaded Microcapsules

The amine encapsulated microcapsules were synthesized by multi-stage emulsion polymerization. The encapsulated corrosion inhibitor particles consist of two parts, a soft inner seed core material and hard outer thermoplastic polymer layer. The inner seed core latex, formed by copolymerization of methyl methacrylate (MMA), butyl acrylate (BA) and methacrylic acid (MA) (MMA:BA:MA = 63:28:9 w/w), was hydrophilic and the average particle size determined by dynamic light scattering (DLS) was 18 nm as shown in Figure 4.6. Due to the hydrophilic characteristics of the acrylate seed, it is difficult to encapsulate by the hydrophobic polystyrene shell with concentric core-shell particle morphology. Therefore, the intermediate shell, with an amphiphilic property, was coated to increase the affinity between the hydrophilic core and the hydrophobic polystyrene (PS) shell. The inner core (18-20 nm) was surrounded by 10 the amphiphilic intermediated shell layer (MMA:BA:MA = 90:7:3 w/w). The outermost hydrophobic layer was composed of polystyrene. After swelling process caused by the diffusion of water and amine through the outer PS polymeric layer, the average thickness of microcapsule was 220 nm. The attraction derived from acid-basic neutralization was used as the driving force to diffuse amine into the core of the capsule. The average particle size (\bar{D}_n) and particle size distribution (PSD) of amine loaded microcapsule are shown in Table 4.1.

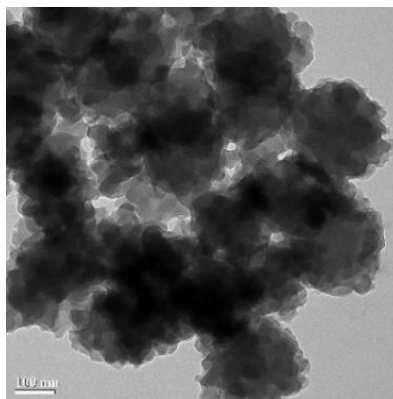
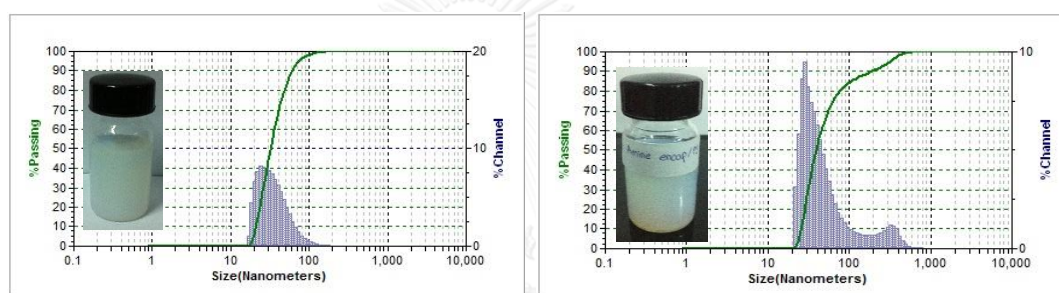
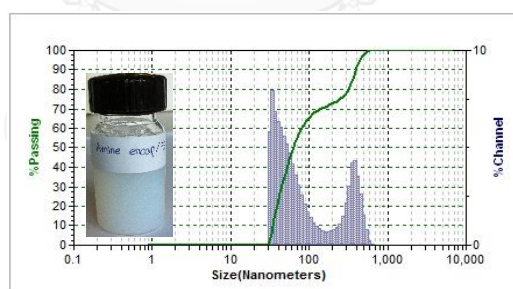


Figure 4.5 Transmission electron micrograph of POT encapsulated in PUF microcapsules containing



(a) Seed core latex

(b) ETA/PS



(c) DEA/PS

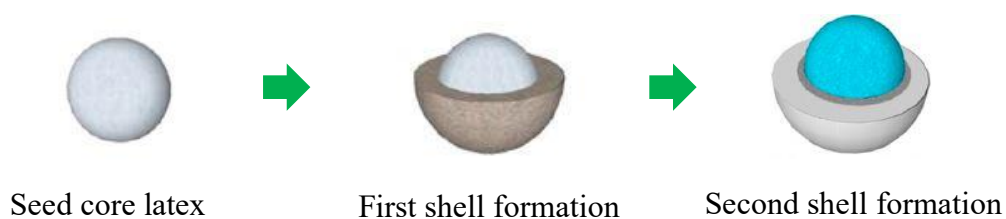


Figure 4.6 Histograms of particle size distribution of (a) seed core latex (b) ETA/PS and (c) DEA/PS

Table 4.2 Amount on silica conversion, solid content, average particle size (\bar{D}_n) and particles size distribution (PSD) of amines encapsulated in polystyrene shell.

Sample	Styrene Conversion (%)	Solid Content (%)	\bar{D}_n (nm)	PSD (nm)
Seed core latex	-	4.9	18.1	5.7
ETA/PS	20.3	10.1	227.8	36.2
DEA/PS	41.5	12.6	212.0	41.9

4.4 Characterization of Self-Healing Hybrid Nanocomposite

The synthesized APTES-modified silica nanoparticles (AMS), GPTMS-modified silica nanoparticles (GMS) and untreated silica nanoparticles were characterized using FTIR spectroscopy. Figure 4.7 shows the FTIR spectra of treated and untreated silica. A weak peak at 690 cm^{-1} and a small peak at 1650 cm^{-1} was observed in AMS spectrum which indicated the existence of amine groups (N–H bending) on the treated silica [28]. The C–N stretching vibration is normally observed in the wave number range $1000\text{--}1200\text{ cm}^{-1}$. However, this peak was not resolved due to the overlay with the IR absorptions of Si–O–Si in the range $1130\text{--}1000\text{ cm}^{-1}$ and of Si–CH₂–R in the range $1250\text{--}1200\text{ cm}^{-1}$. The bands at around $3100\text{--}2800\text{ cm}^{-1}$ associated with the alkyl groups [–(CH₂)_n–] of APTES and GPTMS on the treated surface. The peak of Si–O–Si in the range of $1130\text{--}1000\text{ cm}^{-1}$ in both treated nano-silica indicated that organosilane were successfully grafted on the silica nanoparticles. The broad peak in the region of $3100\text{--}2800\text{ cm}^{-1}$ indicated the alkyl groups [–(CH₂)_n–] of the GPTMS and APTES on the treated surface.

FTIR spectra of self-healing microcapsule, POT and aliphatic amines are shown in Figure 4.8. The spectrum of POT encapsulated capsule showed a peak at 3330 cm^{-1} which indicated the O–H and N–H stretching. A peak at 1620 cm^{-1} and 1540 cm^{-1} represent C–O stretching and N–H bending, respectively, which indicated the formation of PUF from the polymerization between urea and formaldehyde and confirmed the

successful encapsulation of POT as core material. The FTIR spectrum of aliphatic amine encapsulated in polystyrene is shown in Figure 4.8 (b). The peak of O-H stretching at 3390 cm^{-1} was probably due to the presence of moisture on the sample. Peaks at 2916 and 2848 cm^{-1} corresponded to C-H asymmetric and symmetric stretching band, respectively. The peaks at 1462 , 1377 , 1262 , 729 and 719 cm^{-1} corresponded to C-H bending deformation, CH_3 symmetric deformation, twisting deformation and rocking deformation, respectively. The results indicated that the vibration positions belonged to polystyrene which further confirmed the encapsulation of aliphatic amine.

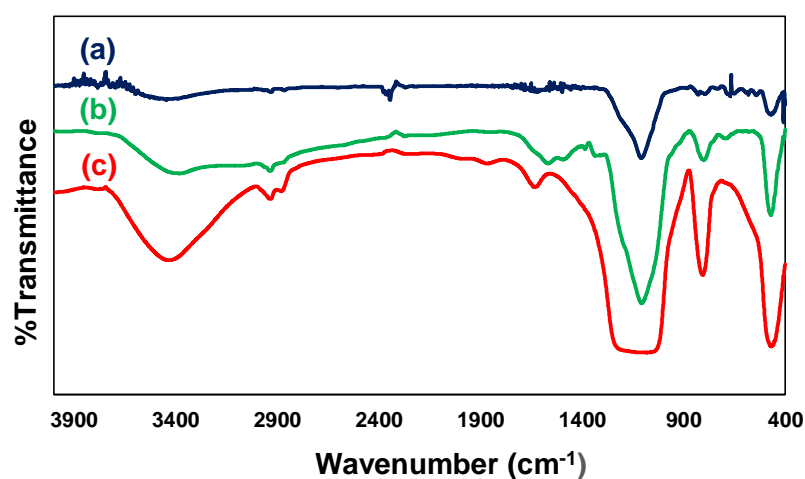


Figure 4.7 FTIR spectra of (a) untreated nano-silica (b) AMS and (c) GMS

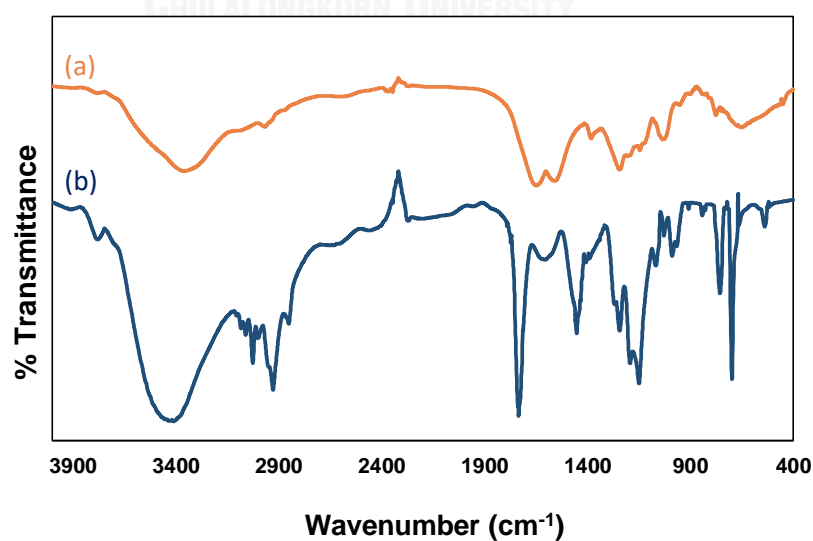


Figure 4.8 FTIR spectra of (a) POT and (b) amines encapsulated in polymer shell

4.5 Dispersion of Silica Nanoparticles in Epoxy Composite

4.5.1 Effect of Curing Agents

The epoxy/ silica hybrid nanocomposite were prepared and coated on microscope slide. The effect of curing agents, tetraethylenepentamine (TEPA) and *p*-phenylenediamine (*p*-PDA), on silica dispersion was investigated. From optical microscope results as shown in Figure 4.9, the dispersion of AMS and GMS slightly change in both TEPA-epoxy and *p*-PDA-epoxy matrix.

4.5.2 Effect of Silica

From optical microscope results, the silica nanoparticles in the nanocomposite reflected light. Thus, the dispersion of the nanoparticles in the polymer matrix could be observed. Figure 4.10 shows the poor dispersion of untreated silica nanoparticles in the polymer matrix and agglomeration when the amount of untreated silica was increased, especially at 5 wt%. The untreated silica nanoparticles were poorly dispersed in a polymer matrix due to the difference in the polarity of untreated silica and epoxy coating. Therefore, the untreated silica nanoparticles tended to agglomerate and form a cluster. From Figure 4.11 APTES-modified silica (AMS) showed well dispersion in the polymer matrix and tend to have less cluster compared to untreated silica nanoparticles. Thus, the amino-modification on the nanoparticles surface dominated the hydrophobic property resulting the good dispersion in a hydrophobicity polymer matrix. Moreover, the amino functional groups on the nanoparticles could bonded with epoxide ring on DGEBA resulting increased film strength.

In addition, Figure 4.11 showed that GPTES modified silica (GMS) also have good dispersion in the polymer matrix even at 5 wt% (magnification of 200X). The contact angle of polymer matrix were investigated to confirm the dispersion of nanoparticles. As shown in Figure 4.12, the contact angle of neat epoxy and epoxy/untreated silica were 61.62 and 73.37, respctively. The contant angle of epoxy/AMS increased to 80.49. Whereas, the contact angle of epoxy/GMS greatly increased to 100.84°. This indicated that the epoxide functional group on the modified-

silica nanoparticles enhanced the hydrophobic property on the nanoparticles surface and enhanced the dispersion of nanoparticles. Moreover, the epoxide functional group on the modified-silica nanoparticles could bonded with amine groups on curing agents resulting increased film strength.

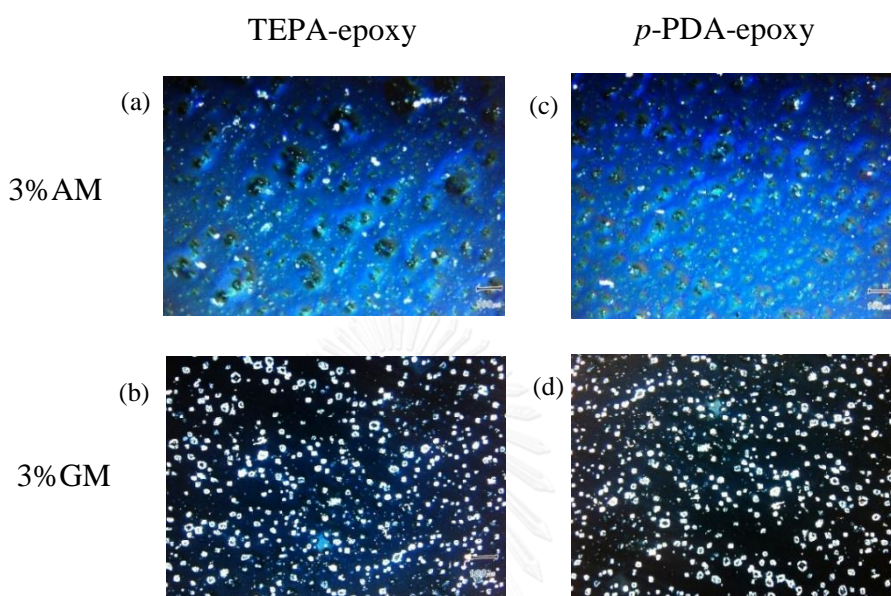


Figure 4.9 Effect of curing agent on nanocomposite (TEPA as curing agent) with (a) 3wt% AMS and (b) 3wt% GMS and nanocompostie (*p*-PDA as curing agent) with (c) 3wt% AMS and (d) 3wt% GMS (magnification of 40X)

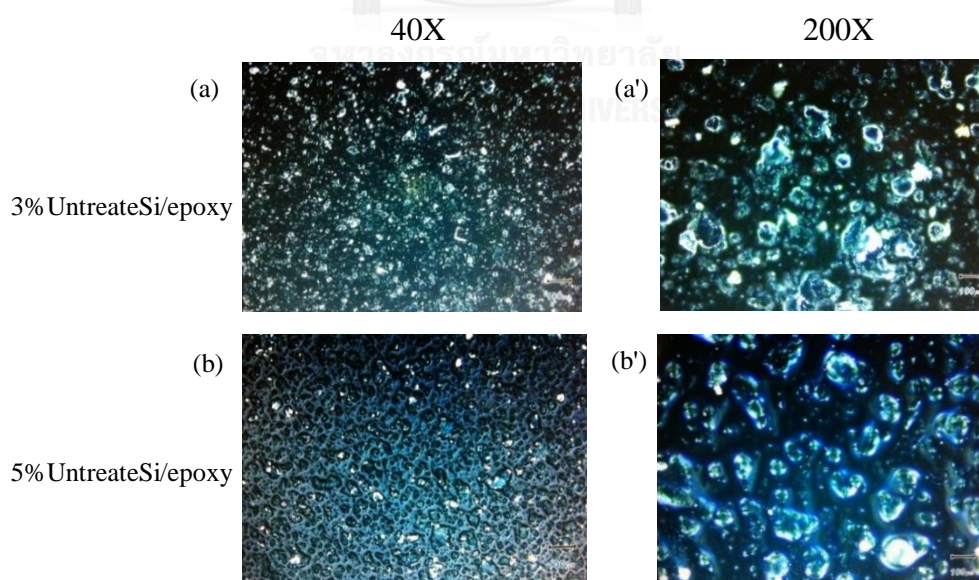


Figure 4.10 Effect of untreated silica loading on the dipersion of silica on 3wt% untreated Si/epoxy (a) 40X, (a') 200X and 5wt% untreated Si/epoxy (b) 40X, (b') 200X (*p*-PDA as curing agent)

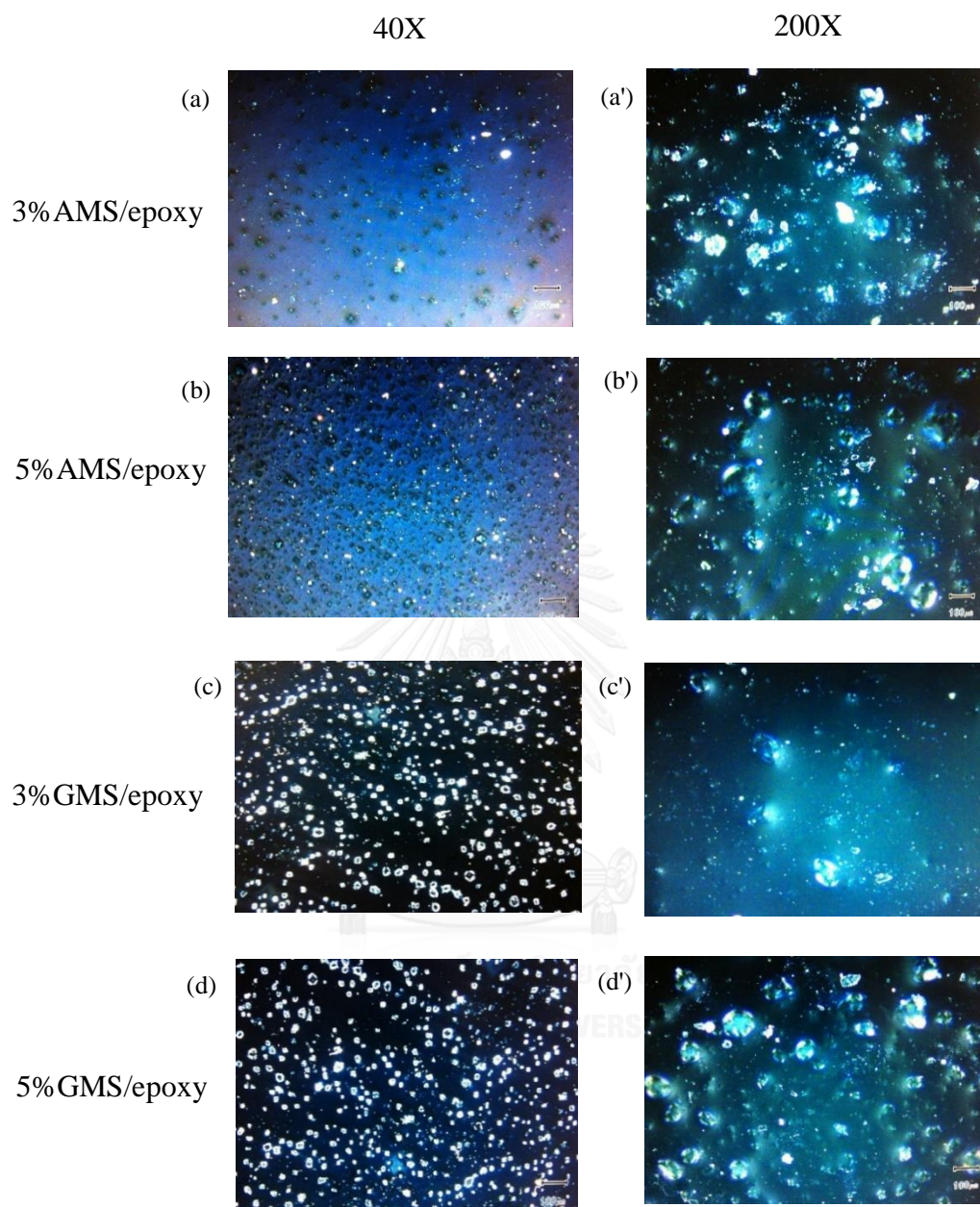


Figure 4.11 Effect of modified silica loading on the dispersion of silica (a) 3wt% AMS/epoxy, (b) 5wt% AMS/epoxy, (c) 3wt% GMS/epoxy, (d) 5wt% GMS/epoxy (at the magnification of 40X) (a', b', c', d' showed magnification at 200X) (*p*-PDA as curing agent)

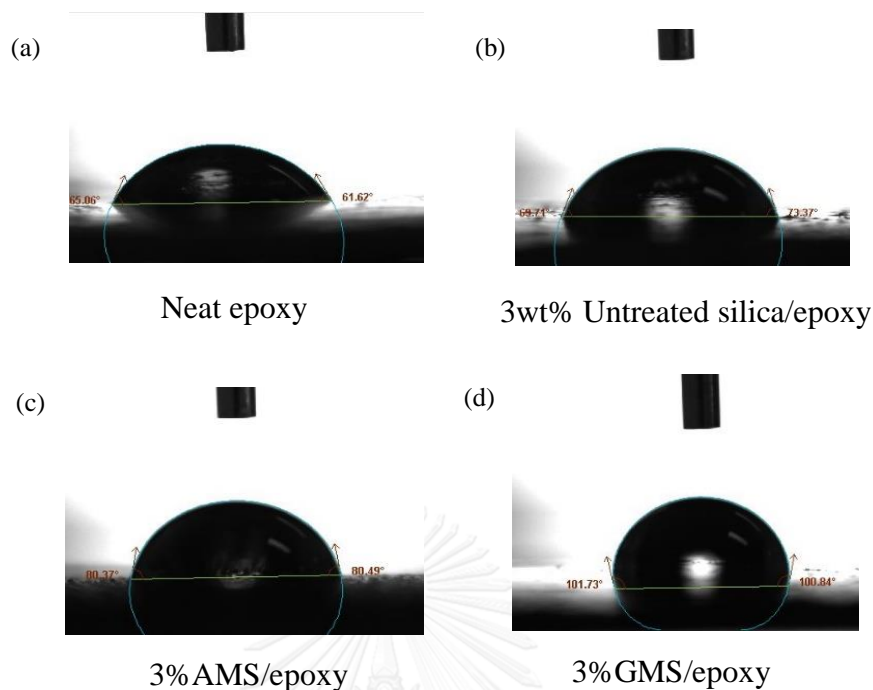


Figure 4.12 Contact angle of (a) neat epoxy, (b) 3wt% Untreated silica/epoxy, (c) 3% AMS/epoxy (d) 3% GMS/epoxy

4.6 Corrosion Studies

4.6.1 Effect of Self-healing Agent

Electrochemical measurement was used to investigate the electrochemical behavior of the epoxy/modified silica/self-healing nanocomposite coated on carbon fiber cloth in 1.0 M H_2SO_4 solution. The effect of self-healing property on anticorrosion performance of composite film was investigated. POT, ETA and DEA encapsulated in microcapsules were incorporated in *p*-PDA-epoxy in the presence of GMS. From Figure 4.13, the cyclic voltammetry of epoxy hybrid nanocomposite incorporated with POT encapsulated microcapsule has the lowest oxidation current (0.6 mA/cm^2) compared with ETA (1.1 mA/cm^2) and DEA (1.075 mA/cm^2) respectively. Therefore, the effect of the amount of POT microcapsule loading (5-20 wt%) on corrosion performance was studied. The result showed that, POT has the highest corrosion

prevention and the anticorrosion performance of epoxy composite increased with increasing amount of self-healing microcapsule.

Table 4.3 Corrosion potential (E_{corr}), corrosion current (I_{corr}), corrosion rate (CR) and % corrosion rate values calculated from Tafel plots for epoxy/modified silica/self-healing nanocomposite samples in 1.0 M H_2SO_4 solution

Sample	Electrochemical measurements			
	E_{corr} (mV)	I_{corr} (mA/cm^2)	R_{corr} (mm/year)	% CR
3%GMS / <i>p</i> -PDA epoxy/10wt%ETA	635.2	0.0141	0.164	0.89
3%GMS / <i>p</i> -PDA epoxy/10wt%DEA	730.4	0.0117	0.136	0.74
3%GMS / <i>p</i> -PDA epoxy/10wt%POT	765.1	0.0079	0.092	0.50

*All samples were 200 μm in thickness

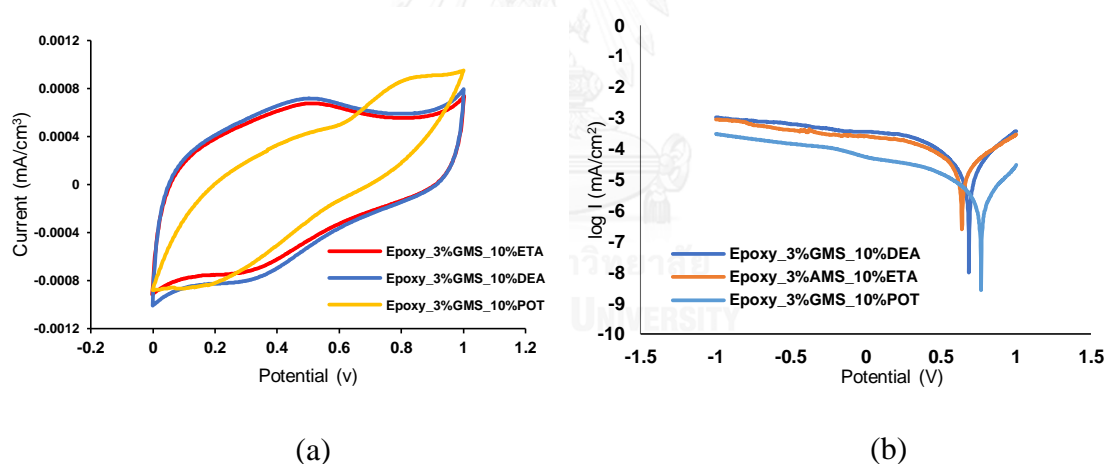


Figure 4.13 Cyclic voltammetry (a) and Tafel plot and (b) of epoxy/modified silica/self-healing nanocomposite with various type of self-healing microcapsule

4.6.2 Effect of Silica Loading and Curing Agents

Neat epoxy film, untreated silica, AMS and GMS incorporated in epoxy film were prepared and characterized. As shown in Fig. 4.14 (a), the electrochemical cyclic voltammetry indicated that the epoxy nanocomposite film coating showed single oxidation peak. Neat epoxy film had the oxidation current (I_{ox}) of 3.81 mA/cm^2 whereas epoxy film incorporated with AMS and GMS had the oxidation current of 2.72 mA/cm^2 and 2.5 mA/cm^2 respectively. The incorporation of GMS in the epoxy matrix significantly increased the anticorrosion performance due to fine dispersion and interaction between silica surface and polymer matrix. The fine dispersion of silica nanocomposite was able to block the diffusion pathway of corrosion agents through the film, resulting to lower corrosion current occurred.

The effect of curing agents, TEPA and *p*-PDA on the anticorrosion performance of hybrid nanocomposite was investigated. Figure 4.14 (b) shows the cyclic voltammetry of TEPA-epoxy and *p*-PDA-epoxy with the incorporated GMS. The *p*-PDA-epoxy incorporated with GMS showed better anticorrosion performance. As previously mention, types of curing agents affect the mechanical properties and chemical resistance properties of nanocomposite. Unlike linear structure of TEPA, the *p*-PDA has benzene ring in its structure which enhances film toughness and chemical resistance. Therefore, *p*-PDA-epoxy incorporated with GMS was used in further study.

The electrochemical Tafel slope analysis was used to identify the anticorrosive performance of epoxy/modified silica/self-healing nanocomposite coating on carbon cloth. Electrochemical Tafel plots for coated epoxy/modified silica/self-healing nanocomposite samples were recorded by sweeping the potential in the range of -1V to $+1\text{V}$ against Ag/AgCl reference electrode in $1.0 \text{ M H}_2\text{SO}_4$ electrolyte. Figure 4.15 shows the Tafel polts for epoxy/silica nanocomposite and epoxy/modified silica/self-healing nanocomposite with various types and amount of curing agents, modified silica and self-healing microcapsules. It was found that the corrosion current decreased with the increasing amount of modified silica, (lowest corrosion current at 3 wt% silica), and self-healing agent. In addition the effect of curing agents, TEPA and *p*-PDA, was also

illustrated. The result showed that *p*-PDA-epoxy composite exhibited lower corrosion current in 1.0 M H₂SO₄ electrolyte.

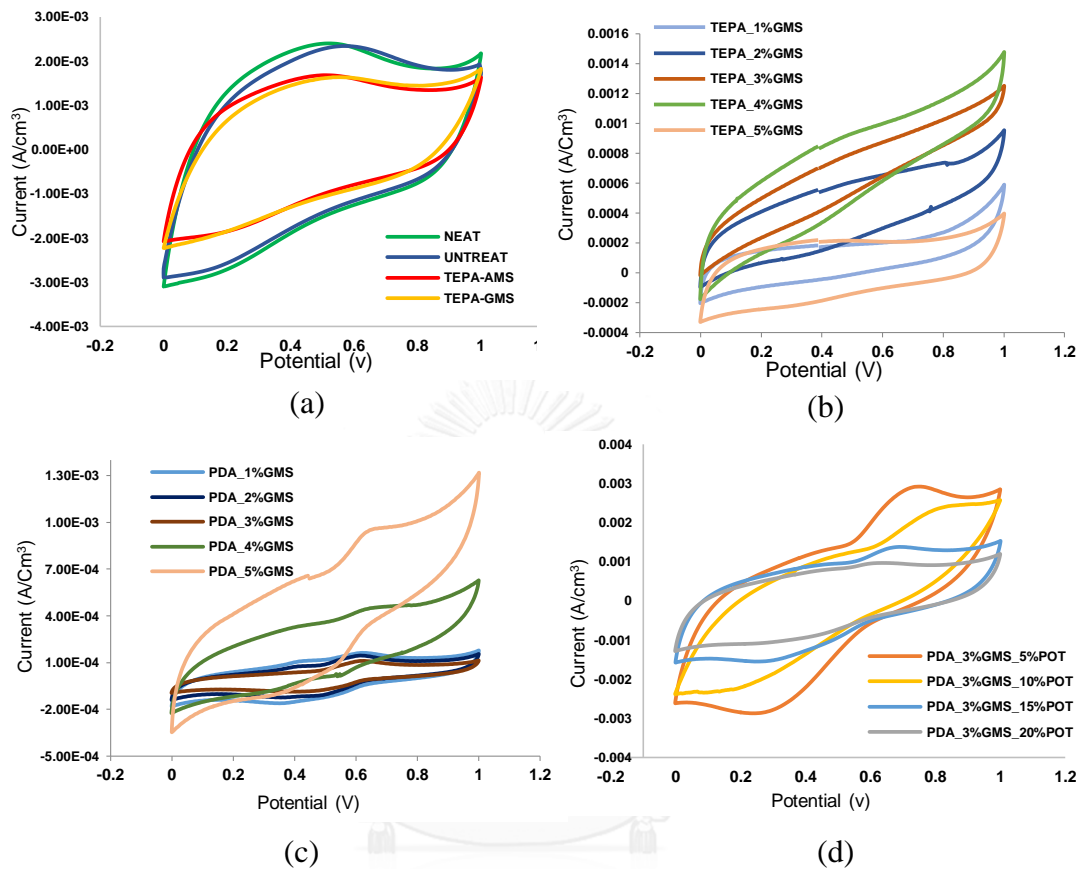


Figure 4.14 Cyclic voltammetry of epoxy nanocomposite with (a) various type of silica (b) various amount of silica in TEPA-epoxy (c) various amount of silica in *p*-PDA-epoxy and (d) various amount of POT microcapsules

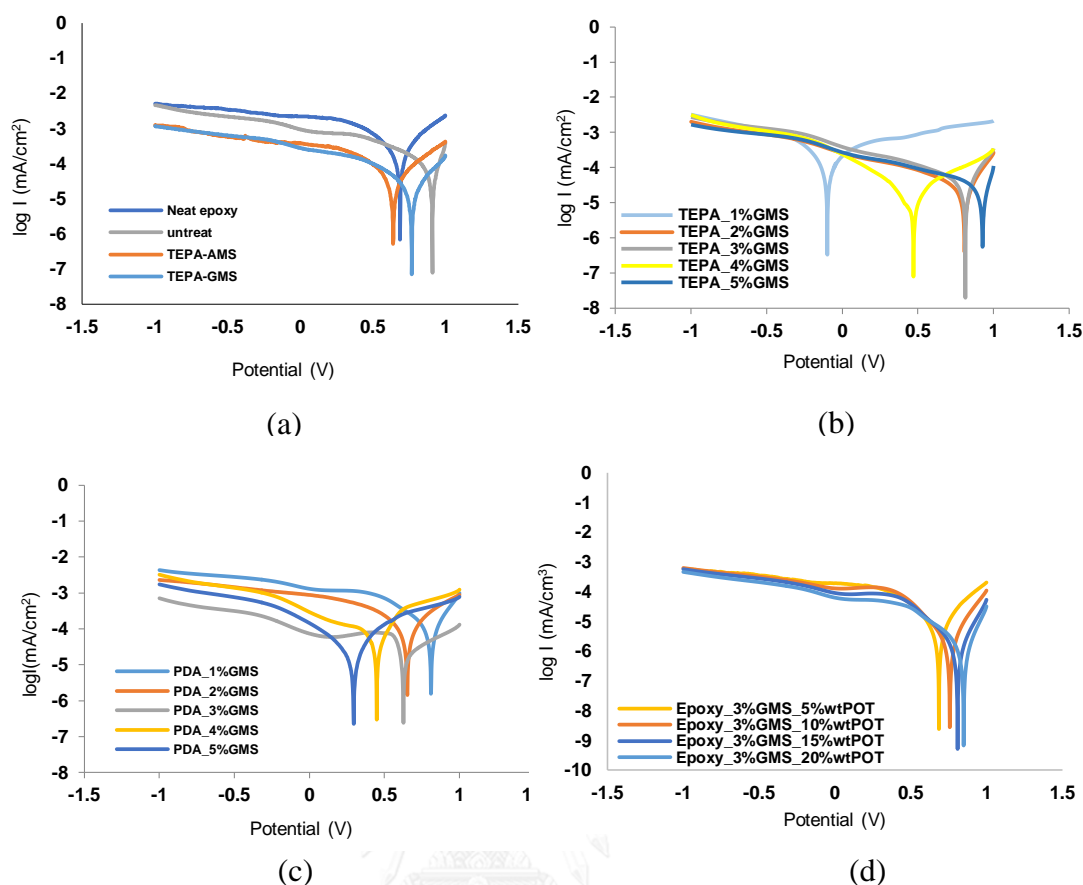


Figure 4.15 Scanning Tafel plots for epoxy nanocomposite with (a) various type of silica (b) various amount of silica in TEPA-epoxy (c) various amount of silica in *p*-PDA –epoxy and (d) various amount of POT microcapsules

Table 4.4 presents the corrosion potential (E_{corr}), corrosion current (I_{corr}), corrosion rate (CR) and % corrosion rate calculated from Tafel plots of coated samples in 1.0 M H₂SO₄. From the calculated data, it can be seen that the corrosion rate and % CR of epoxy/modified silica nanocomposite coated samples were much lower than neat epoxy coated sample. Thus, the incorporation of modified silica nanoparticles, especially GMS, in epoxy matrix promoted the anticorrosive efficiency of coated steel samples by blocking the diffusion pathway of corrosive agents and decreased in wettability. For wt% of modified silica loading, the corrosion rate decreased with increasing of modified silica loading. The similar behavior was observed for the incorporation of self-healing microcapsules in epoxy matrix, corrosion rate decreased with increasing of self-healing microcapsules loading.

Comparison of the corrosion rate of epoxy/modified silica nanocomposite and epoxy/modified silica/self-healing nanocomposite coated with various modified silica and self-healing microcapsule loadings showed that the anticorrosion performance of epoxy/modified silica/self-healing nanocomposite coating with 3 wt% of GMS and 20 wt% of POT exhibited lowest corrosion rate for all coating samples. The corrosion protection of epoxy/modified silica/self-healing nanocomposite was dramatically enhanced compared to neat epoxy coated samples. The anticorrosion performance was enhanced not only by the well dispersed GMS on the epoxy matrix but POT microcapsules also had an important role in healing film crack caused by corrosive environment. When the crack occurred on the coated films and broke the outer shell of the microcapsule, self-healing agent (POT) leaked and hydrolyzed in wet environment to form a hydrophobic silane crosslink network. The newly form films has hydrophobic properties due to the fluorine on POT structure. The newly form hydrophobic film helped enhanced the anticorrosion performance. Therefore, corrosion rate and % CR could be decreased by increasing self-healing microcapsules loading.

Figure 4.16 also shows that the % corrosion rate decreased with incorporated of modified silica and self-healing microcapsule into epoxy polymer. Therefore, the corrosion protection of epoxy/modified silica/self-healing nanocomposite is better than neat epoxy coated samples.

Table 4.4 Corrosion potential (E_{corr}), corrosion current (I_{corr}), corrosion rate (CR) and % corrosion rate values calculated from Tafel plots for epoxy/modified silica nanocomposite and epoxy/modified silica/self-healing nanocomposite samples in 1M H_2SO_4 solution

Sample	Electrochemical measurements			
	E_{corr} (mV)	I_{corr} (mA/cm ²)	R_{corr} (mm/year)	% CR
Neat epoxy	682	1.584	18.374	100.00
Untreated silica/epoxy	730.4	0.632	7.331	39.90
1%GMS /TEPA-epoxy	98.8	0.361	4.188	22.79
2%GMS /TEPA-epoxy	807.6	0.315	3.654	19.89
3%GMS /TEPA-epoxy	470.5	0.267	3.097	16.86
4%GMS /TEPA-epoxy	813.5	0.275	3.190	17.36
5%GMS /TEPA-epoxy	928.6	0.283	3.283	17.87
1%GMS / <i>p</i> -PDA-epoxy	809.6	0.158	1.833	9.97
2%GMS / <i>p</i> -PDA-epoxy	628.3	0.135	1.566	8.52
3%GMS / <i>p</i> -PDA-epoxy	626.3	0.117	1.357	7.39
4%GMS / <i>p</i> -PDA-epoxy	448.6	0.124	1.438	7.83
5%GMS / <i>p</i> -PDA-epoxy	293.8	0.13	1.508	8.21
3%GMS / <i>p</i> -PDA epoxy/5wt%POT	737.3	0.104	1.206	6.57
3%GMS / <i>p</i> -PDA epoxy/10wt%POT	761.8	0.063	0.731	3.98
3%GMS / <i>p</i> -PDA epoxy/15wt%POT	792.1	0.037	0.429	2.34
3%GMS / <i>p</i> -PDA epoxy/20wt%POT	851.4	0.012	0.139	0.76

*All sample were 50 μm in thickness

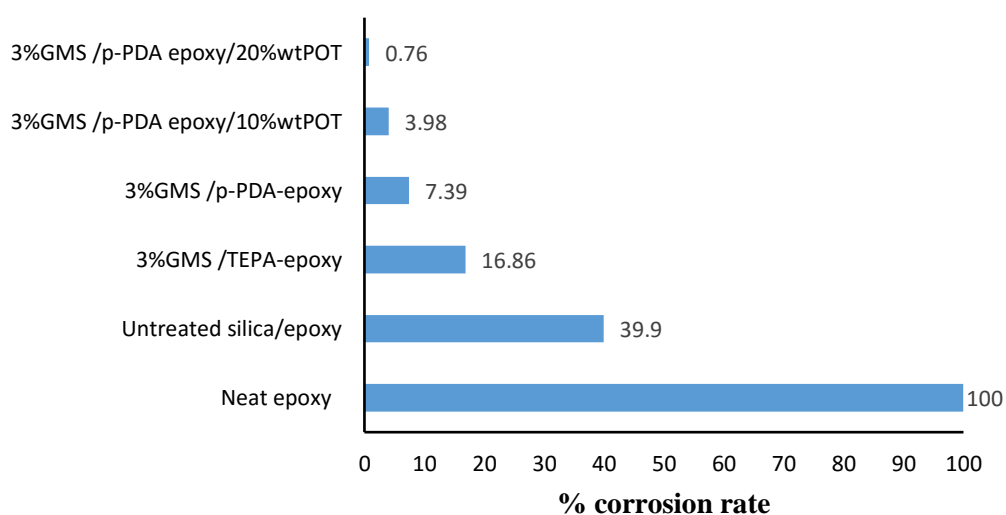


Figure 4.16 Corrosion rate of neat epoxy and epoxy/silica nanocomposite with various types of curing agents and POT loading at 10 and 20 wt%

4.7 Salt Spray Test

Figure 4.17 show the specimens of coated cold-rolled steel with epoxy/modified silica/self-healing nanocomposite modified with GMS at 1-5 wt% and self-healing microcapsules at 5-25 wt% before and after the salt spray test for 97 hours. The coated film on the cold-rolled steel specimens were cut cross as X-mark according to ASTM 1654 (Standard test method for evaluation of painted or coated specimens subjected to corrosive Environments) before the salt spray test. The surface of epoxy/modified silica nanocomposite (1-5wt% GMS) as shown in Figure 4.17 (e)-(i) was rapidly rusted around the X-mark cross due to the flaw and crack of the coated film. From Figure 4.17 (a)-(d), the epoxy/modified silica nanocomposite with the incorporated POT (5-25wt% %) as self-healing agent shows less rusted area around the cut on the film surface. The result showed that GMS incorporated in epoxy matrix could enhance the mechanical properties and anticorrosion performance but did not significantly protect the steel substrate after the film was flawed. However, by adding POT as self-healing agents into epoxy hybrid nanocomposite, the anticorrosion performance increased significantly. The rusty area on coated film samples were measured and shown as rating number representing the mean creepage according to ASTM 1654 as showed in Table 4.5

Table 4.5 Rating of failure according to ASTM 1654

Sample	Average rust occurred (mm)	Rating number
3%GMS / <i>p</i> -PDA epoxy/5wt%POT	0.84	8
3%GMS / <i>p</i> -PDA epoxy/10wt%POT	0.63	8
3%GMS / <i>p</i> -PDA epoxy/15wt%POT	0.45	9
3%GMS / <i>p</i> -PDA epoxy/20wt%POT	0.30	9
1%GMS / <i>p</i> -PDA-epoxy	3.86	5
2%GMS / <i>p</i> -PDA-epoxy	2.36	6
3%GMS / <i>p</i> -PDA-epoxy	0.72	8
4%GMS / <i>p</i> -PDA-epoxy	1.58	7
5%GMS / <i>p</i> -PDA-epoxy	2.84	6

*All sample were 50 μ m in thickness

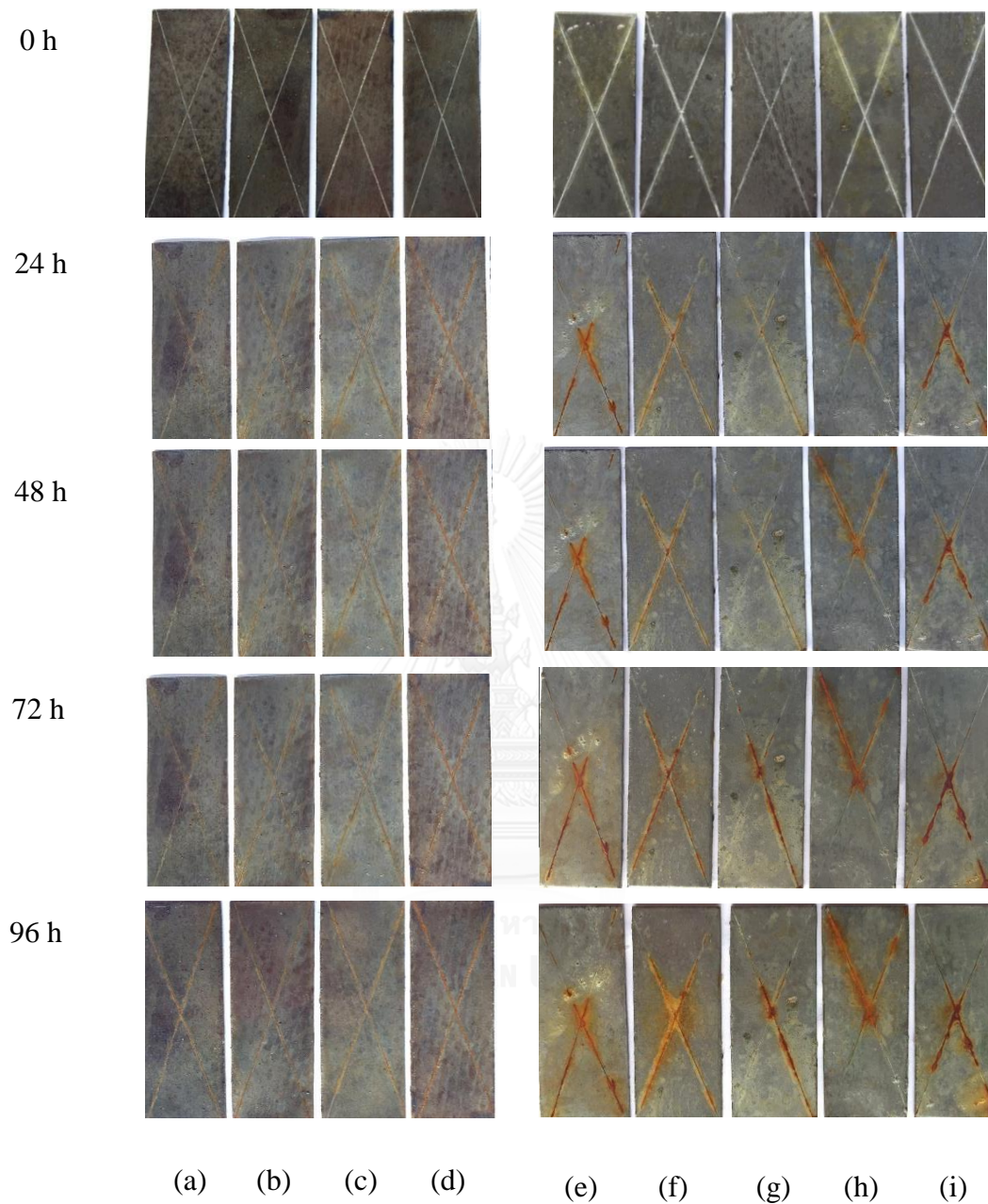


Figure 4.17 Coupons of coated steel of epoxy/modified silica/self-healing nanocomposite coating after salt spray test for 0, 24, 48 72 and 96 h; *p*-PDA-epoxy/3wt%GMS nanocomposite with the incorporate of (a) 5wt% POT, (b) 10wt% POT, (c) 15wt% POT, (d) 20wt% POT and *p*-PDA-epoxy incorporate with (e) 1wt% GMS, (f) 2wt% GMS , (g) 3wt% GMS , (h) 4wt% GMS and (i) 5wt% GMS.

4.8 Morphology of Epoxy/Modified silica/Self-Healing Nanocomposite on Steel

The surface morphologies and self-healing performance of the polymeric films of epoxy/modified silica/self-healing nanocomposite were characterized by scanning electron microscopy (SEM). As shown in Figure 4.18, the surface of the epoxy/modified silica/self-healing nanocomposite films with 50 μm thickness were smooth before the corrosion test. According to ASTM D 1645, the cut area was observed to study self-healing performance of epoxy/3wt%GMS film incorporated with POT and DEA under corrosive environment. From Figure 4.18 (a') and (b'), after 96 h of salt spray test, composite films surfaces were rough which indicated the corrosion of epoxy film. Epoxy/3wt%GMS/20wt%POT showed a flatten cut area due to the new layer of silane crosslink network formed by POT. For epoxy/3wt%GMS/20wt%DEA, the new layer was not observe because on crosslink network was formed but only neutralized of amine with acid.

The healing mechanism of POT is represented in Figure 4.19. After the nanocomposite film exposed in corrosive environment for long period of time, film started to erode and crack occurred. Self-healing microcapsules shell broke due to the crack and POT leaked from the microcapsules to the damage area. In wet environment, POT can self-hydrolyzed and form a crosslink network of silane-base film. The newly formed film from hydrolysis and poly-condensation of POT and water is hydrophobic, indicating a special wetting property which would serve to repel aqueous electrolyte solution away from metal and to provide further corrosion protection to cold-rolled steel substrate.

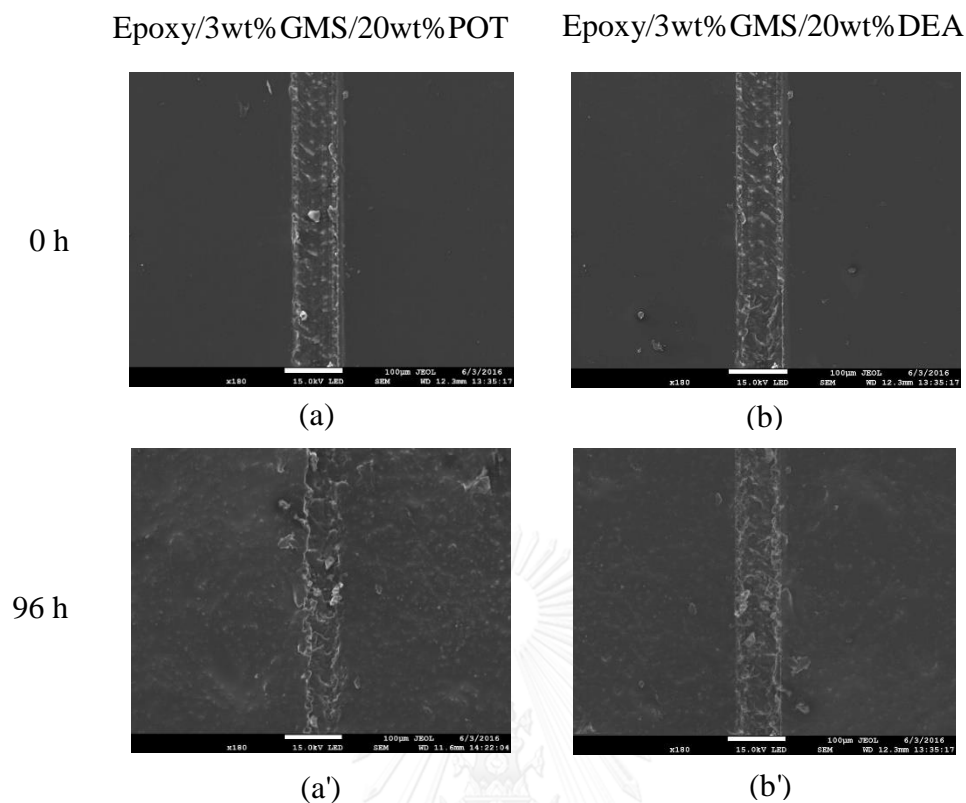


Figure 4.18 SEM images of surface area of (a) epoxy/3wt%GMS/20%POT and (b) epoxy/3wt%GMS/20%DEA nanocomposite coating (50 µm thickness) before corrosion test, (a') and (b') showed nanocomposite coating after corrosion test (180X magnification)

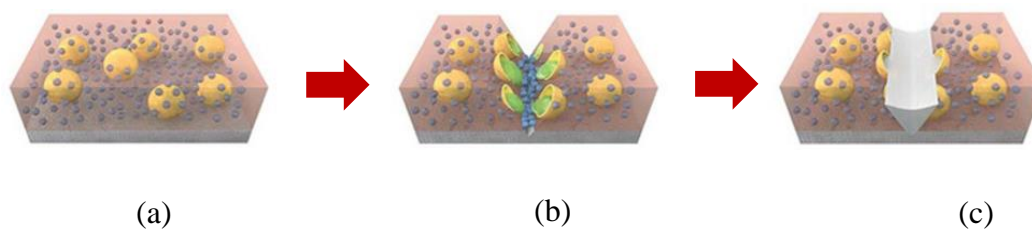


Figure 4.19 Self-healing mechanism of epoxy/GMS/POT coatings; (a) before exposed in corrosive environment, (b) during corrosion process and (c) new film layer obtained by POT. (B.J. Blaiszik, Self-Healing Polymers and Composites)

CHAPTER V

CONCLUSIONS AND SUGGESTIONS

5.1 Conclusions

Epoxy/modified silica/self-healing hybrid nanocomposite coating was successfully prepared and the effect of curing agents, modified silica nanoparticles and self-healing microcapsule was investigated. APTES and GPTES were used to modify the surface of silica nanoparticles, whereas, POT, ETA and DEA were used as self-healing agents to enhance the corrosion resistance of epoxy coating. The FTIR result indicated that the organosilane were successfully grafted on the silica nanoparticles.

Modified silica nanoparticles were then incorporated into the polymer matrix. Optical microscope result showed that AMS and GMS were successfully dispersed in polymer matrix, especially GMS which showed less agglomeration compared to AMS and unmodified silica nanoparticles. Good dispersion of silica in polymer matrix led to an increment corrosion resistance due to the obstruction of water and oxygen diffusion pathway.

The electrochemical measurements showed that the incorporation of modified silica nanoparticles significantly enhanced the anticorrosion performance of epoxy coating. Moreover, the addition of self-healing microcapsules into epoxy polymer greatly decreased the corrosion rate of hybrid nanocomposite. From salt spray result, the corrosion protection increased significantly. Epoxy hybrid nanocomposite with the incorporated GMS and POT showed good anticorrosion performance for 96 hours of salt spray test and achieved the rating number of 9 according to ASTM D1654. Therefore, epoxy/3%GMS/20wt%POT coating showed best corrosion resistance performance.

5.2 Suggestions of the Future Work

A future investigation of epoxy/ modified silica/ self-healing nanocomposite should be carried out with the following aspects:

1. Synthesis of epoxy/ modified silica/ self-healing nanocomposite
 - The synthesis of epoxy hybrid nanocomposite using different type of curing agents
 - The effect of various filler e.g. SiO₂, TiO₂, CNT in epoxy matrix
2. Application of epoxy/ modified silica/ self-healing nanocomposite
 - The preparation of epoxy/ modified silica/ self-healing nanocomposite with enhanced the mechanical properties and gas barrier properties (permeability of film)

REFERENCES

1. McAdams, L.V., and Gannon, J.A., *High Performance Polymers and Composite* (1st edition, Kroschwitz J., 1991), p. 258-318.
2. May, C.A., *Epoxy Resins Chemistry and Technology* (2nd edition, Marcel Dekker Inc,1988), p.38.
3. McGarry, F.J., *Polymer Toughening* (1st edition, Arends C. B., 1996), p. 175-188.
4. Zhao, Y., Zhang, W., *Self-healing coatings containing microcapsule* (Appl. Surf. Sci., 2012), p. 1915-1918.
5. Shaw, S.J., *Rubber Toughened Engineering Plastics* (Netherlands: Arends C. B., 1994), p. 165-209.
6. Tesoro, G., *Epoxy Resins: Chemistry and Technology* (Marcel Dekker Inc., 1987), p.201-205.
7. Hedrick, J., Yilgor, I., Wilkes, G., *Toughening of Epoxy Resins with Ductile Glassy Thermoplastics* (Polymer Bulletin, 1985), p. 201-208.
8. Sun, Y., Zhang, Z., and Wong, C.P., Study on mono-dispersed nano-size silica by surface modification for underfill applications, *Colloid Interface Sci. J.*, 292, (2005): p. 436-44.
9. Roussi, E., Tsetsekou, A., Skarmoutsou, A., Anticorrosion and nanomechanical performance of hybrid organo-silicate coatings integrating corrosion inhibitors, *Surf. Coat. Technol. J.*, 232, (2013): p. 131-141.
10. Zou, H., Wu, S., and Shen, J., Polymer/silica nanocomposite: preparation, characterization, properties, and applications, *Chem. Rev. J.*, 108, (2008): p. 3893-3957.
11. Stojanovic, D.B., Brajovic, L., Orlovic, A., Transparent PMMA/silica nanocomposite containing silica nanoparticles coating under supercritical conditions, *Prog. Org. Coat.*, 76, (2013): p. 626–631.
12. Isin, D., Kayaman, A.N., and Güngör, A., Preparation and characterization of UV-curable epoxy/silica nanocomposite coatings, *Prog. Org. Coat.*, 65 (2009): p. 477–483.

13. Türünç, O., Menciloglu, Y., Güngör, A., Nonisocyanate based polyurethane/silica nanocomposite and their coating performance. *Sol-Gel Sci. Technol.*, 47, (2008): p. 290–299.
14. Watanabe, M., and Tamai, T., Sol-gel reaction in acrylic polymer emulsions: the effect of particle surface charge, *Sol-Gel Sci. Technol.*, 23, (2007): p. 3062–6.
15. Weng, C.J., Jhuo, Y.S, Yi, L., Advanced antistatic/anticorrosion coatings prepared from polystyrene composite incorporating dodecylbenzenesulfonic acid-doped SiO₂@polyaniline core–shell microspheres. *Polym. Int.*, 62, (2013): p. 774–782.
16. Nazir, T., Afzal, A., Siddiqi, H.M., Thermally and mechanically superior hybrid epoxy-silica polymer films via sol-gel method. *Prog. Org. Coat.*, 69, (2010): p. 100–106.
17. Nakamura, Y., Yamaguchi, M., Okubo, T., Effect of particle size on impact properties of epoxy resin filled with angular shaped silica particles, *Polymer*, 32, (1992): p. 1281.
18. Salomone, J.C., *Encyclopedia of polymeric materials*, (Marcel Dekker Inc, 1996), p.632-645
19. Nielsen, L.E., *Mechanical properties of polymers and composite*, (New York:1974), p. 745-760
20. Ochi, M., and Matsumura, T., Polymer Physics, *J. Polym. Sci.*, 43, (2006): p. 1631-1639.
21. Mascia, L., Prezzi, L., and Haworth, B., *Hybrid Nanocomposites for Nanotechnology: Electronic, Optical, Magnetic and Biomedical Applications*, (Springer Science & Business, 2006), p. 1145-1155.
22. Matejka, L., Dukh, O., Drahomira, H., Preparation and Characterization of Hybrid Organic-Inorganic Epoxide-Based Films and Coatings Prepared by the Sol-Gel Process, *Macromolecules*, 34, (2001): p. 6904-6914.
23. Jack, T.R., Wilmott, M.J., Sutherby, R.L., *External corrosion of line pipe - A summary of research activities*, (New York:1996), p.18-24.
24. Wagner, C., *Corrosion in aqueous solution and corrosion in gases at elevated temperature—analogies and disparities*, (Werkst. Korros, 1974), p. 161–165.

25. Ghosh, S.K., *Self-healing Materials: Fundamentals, Design Strategies, and Applications*, (Wiley-VCH, 2008), p. 692-719
26. Feng, W., Patel, S.H., Young, M.Y., Smart polymeric coatings - Recent advances, *Adv. Polym. Tech. J.*, 26, (2007): p. 1-13.
27. Huang, T.C., Su, Y.A., and. Yeh, T.C., Advanced anticorrosive coatings prepared from electroactive epoxy-SiO₂ hybrid nanocomposite materials, *Electrochimica Acta.*, 56, (2011): p. 6142- 6149.
28. Ghanbari, A., and Attar, M.M., A study on the anticorrosion performance of epoxy nanocomposite coatings containing epoxy-silane treated nano-silica on mild steel substrate, *J. Ind. and Eng.Chem.*, 23, (2015): p. 145-153.
29. Huang, M., Zhang, H., and Yang, J., Synthesis of organic silane microcapsules for self-healing corrosion resistant polymer coatings, *Corr. Sci. J.*, 65, (2012): p. 561-566.
30. Choi, H., and Kim, K., Encapsulation of aliphatic amines into nanoparticles for self-healing corrosion protection of steel sheets. *Prog. Org. Coat.*, 76, (2013): p. 1316-1324.
31. Choi, H., White, S.R., Braun, P.V., Encapsulation of triethanolamine as organic corrosion inhibitor into nanoparticles and its active corrosion protection for steel sheets, *Surf & Coat Tech*, 206, (2012): p. 2354-2362.
32. Kumar, A., Stephenson, L.D., and Murray, J.N., Self-healing coatings for steel, *Prog Org Coat*, 55, (2006): p. 244-253.
33. Brown E.N., White, S.R., In situ poly(urea-formaldehyde) microencapsulation of dicyclopentadiene, *J. Microencap*, 43, (2003): p.2347-2353
34. Langea, J., Wu, S.S., Influence of structure and chemical composition on oxygen permeability of crosslinked epoxy-amine coatings, *Polymer*, 5, (2002): p. 985-5994.
35. Wetzal, B., Rosso, P., Hauptert, F., Epoxy nanocomposite – fracture and toughening mechanisms. *Eng. Frac. Mech.*, 73, (2006): p. 2375-2398.
36. Hofen, K., and Weber, S., Novel titration method for surface-functionalised silica. *App. Surf. Sci.*, 257, (2011): p. 2576-2580.

APPENDIX

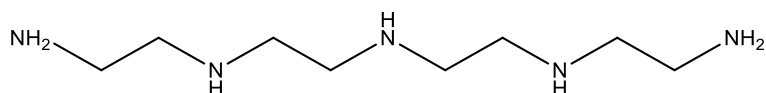


จุฬาลงกรณ์มหาวิทยาลัย
CHULALONGKORN UNIVERSITY

Appendix A

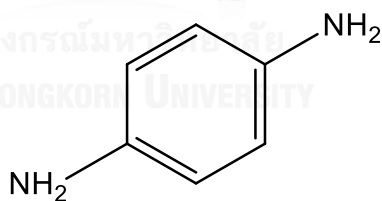
The Properties of Curing Agents, Self-Healing Agents, Fume Silica and Chemical Composition of the Steel Samples

Table A-1 Properties of Tetraethylenepentamine (TEPA)

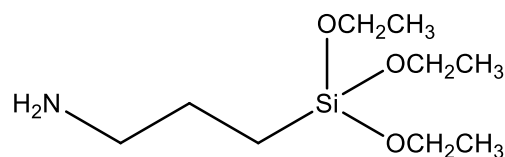


Properties	Tetraethylenepentamine
Molecular formula	$C_8H_{23}N_5$
Molar mass	189.3 g/mol
Density	0.991 g/cm ³
Melting point	-30°C
Boiling point	332°C
Appearance	Yellow viscous liquid
Physical form	Viscous liquid
Vapor pressure, 25 °C	<0.01 mmHg

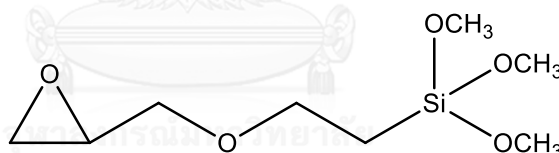
Table A-2 Properties of para-Phenylenediamine (*p*-PDA)



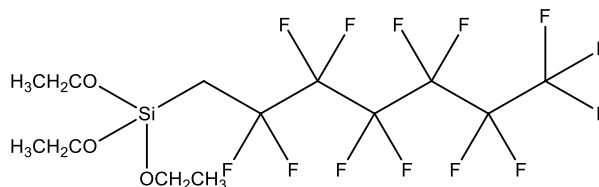
Properties	<i>para</i> -Phenylenediamine
Molecular formula	$C_6H_4(NH_2)_2$
Molar mass	108.14 g/mol
Density	>1 g/cm ³
Melting point	145°C
Boiling point	267°C
Appearance	White crystalline solid
Physical form	Crystalline solid
Vapor pressure, 25 °C	<0.01 mmHg

Table A-3 Properties of (3-Aminopropyl)triethoxysilane (APTES)

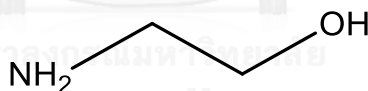
Properties	(3-Aminopropyl)triethoxysilane
Molecular formula	$C_9H_{23}NO_3Si$
Molar mass	221.37 g/mol
Density	0.942 g/cm^3
Melting point	-70°C
Boiling point	217°C
Appearance	Clear liquid
Physical form	Liquid
Vapor pressure, 25°C	$<0.01 \text{ mmHg}$

Table A-4 Properties of 3-Glycidyloxypropyl)trimethoxysilane (GPTMS)

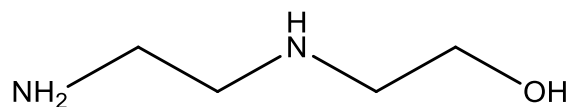
Properties	3-Glycidyloxypropyl)trimethoxysilane
Molecular formula	$C_9H_{20}O_5Si$
Molar mass	196.34 g/mol
Density	1.07 g/cm^3
Melting point	0°C
Boiling point	290°C
Appearance	Transparent liquid
Physical form	Liquid
Vapor pressure, 25°C	0.0142 mmHg

Table A-5 Properties of Perfluorooctyltriethoxysilane (POT)

Properties	Perfluorooctyltriethoxysilane
Molecular formula	$C_{14}H_{19}F_{13}O_3Si$
Molar mass	510.36 g/mol
Density	1.64 g/cm ³
Melting point	-38°C
Boiling point	95°C
Appearance	Clear liquid
Physical form	Liquid
Vapor pressure, 25 °C	<0.01 mmHg

Table A-6 Properties of Ethanolamine (ETA)

Properties	Ethanolamine
Molecular formula	C_2H_7NO
Molar mass	61.08 g/mol
Density	1.012 g/cm ³
Melting point	10°C
Boiling point	170°C
Appearance	Clear liquid
Physical form	Liquid
Vapor pressure, 20 °C	0.48mmHg

Table A-6 Properties of Diethanolamine (DEA)

Properties	Diethanolamine
Molecular formula	C ₄ H ₁₁ NO ₂
Molar mass	105.14 g/mol
Density	1.094 g/cm ³
Melting point	-6°C
Boiling point	127°C
Appearance	Colorless to yellow liquid
Physical form	Liquid
Vapor pressure, 20 °C	<0.1 mmHg

Table A-7 Chemical composition of the cold-rolled steel.

Element	Percent (w/w, %)
Fe	99.72
Mn	0.18
C	0.1

Appendix B

Calculation of Rating Number (ASTM D 1654)

Table B.1 Rating number calculation and standard deviation

Experiment	Rust formed (mm)						Total
	area1	area2	area3	area4	area5	area6	
1%GMS / <i>p</i> -PDA-epoxy	4.5	3.9	3.6	4.1	3.9	3.6	3.93
1%GMS / <i>p</i> -PDA-epoxy	3.5	4.2	4.3	3.6	4.2	3.4	3.87
1%GMS / <i>p</i> -PDA-epoxy	3.2	4.1	3.6	3.7	4.2	3.8	3.77
Mean							3.86
Rating number							5
2%GMS / <i>p</i> -PDA-epoxy	2.2	2.3	2.5	3.1	2.7	2.0	2.47
2%GMS / <i>p</i> -PDA-epoxy	2.7	2.5	2.6	1.5	3.5	1.1	2.32
2%GMS / <i>p</i> -PDA-epoxy	3.1	2.3	1.8	2.8	1.0	2.8	2.30
Mean							2.36
Rating number							5
3%GMS / <i>p</i> -PDA-epoxy	1.1	0.5	0.8	0.7	0.7	0.6	0.73
3%GMS / <i>p</i> -PDA-epoxy	0.4	0.6	0.5	1.0	0.5	0.8	0.63
3%GMS / <i>p</i> -PDA-epoxy	1.2	0.8	0.6	0.7	0.4	1.1	0.80
Mean							0.72
Rating number							8
4%GMS / <i>p</i> -PDA-epoxy	1.9	1.7	1.7	1.3	1.9	1.7	1.70
4%GMS / <i>p</i> -PDA-epoxy	1.5	1.8	1.8	1.5	1.3	0.8	1.45
4%GMS / <i>p</i> -PDA-epoxy	1.6	1.5	1.8	1.4	1.6	1.7	1.60
Mean							1.58
Rating number							7
5%GMS / <i>p</i> -PDA-epoxy	2.5	3.1	3.0	2.9	2.1	2.4	2.67
5%GMS / <i>p</i> -PDA-epoxy	3.2	2.5	2.9	3.8	3.5	4.1	3.33
5%GMS / <i>p</i> -PDA-epoxy	2.7	2.5	1.9	2.7	2.9	2.4	2.52
Mean							2.84
Rating number							6

Table B.1 Rating number calculation and standard deviation (continued)

Experiment	Rust formed (mm)						Total
	area1	area2	area3	area4	area5	area6	
3%GMS /p-PDA epoxy/5wt%POT	0.9	1.0	0.7	0.8	0.6	1.2	0.87
3%GMS /p-PDA epoxy/5wt%POT	1.0	1.1	0.8	0.4	0.8	1.0	0.85
3%GMS /p-PDA epoxy/5wt%POT	1.1	0.8	0.6	0.5	1.3	0.5	0.80
Mean							0.84
Rating number							8
3%GMS /p-PDA epoxy/10wt%POT	0.5	0.5	0.6	0.9	0.6	0.7	0.63
3%GMS /p-PDA epoxy/10wt%POT	0.7	1.0	0.4	0.7	0.4	0.9	0.68
3%GMS /p-PDA epoxy/10wt%POT	0.5	0.6	0.5	0.7	0.4	0.8	0.58
Mean							0.63
Rating number							8
3%GMS /p-PDA epoxy/15wt%POT	0.3	0.4	0.6	0.7	0.5	0.6	0.52
3%GMS /p-PDA epoxy/15wt%POT	0.3	0.6	0.3	0.2	0.5	0.4	0.38
3%GMS /p-PDA epoxy/15wt%POT	0.7	0.5	0.7	0.5	0.6	0.4	0.57
Mean							0.49
Rating number							9
3%GMS /p-PDA epoxy/20wt%POT	0.3	0.5	0.4	0.3	0.2	0.1	0.30
3%GMS /p-PDA epoxy/20wt%POT	0.1	0.3	0.6	0.4	0.5	0.2	0.35
3%GMS /p-PDA epoxy/20wt%POT	0.3	0.2	0.4	0.5	0.3	0.2	0.32
Mean							0.32
Rating number							9

Appendix C

Appearance of coated nanocomposite on microscope slide and CRS

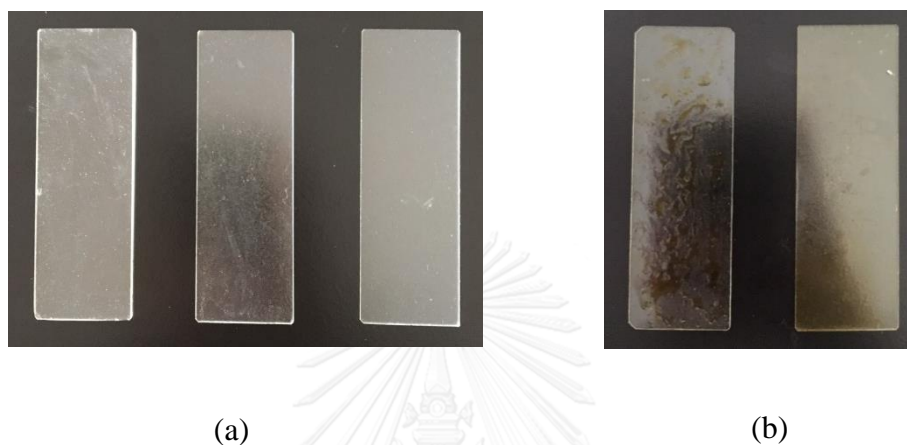


Figure C.1 Appearance of (a) TEPA-epoxy/GMS (white) and (b) p-PDA-epoxy/GMS

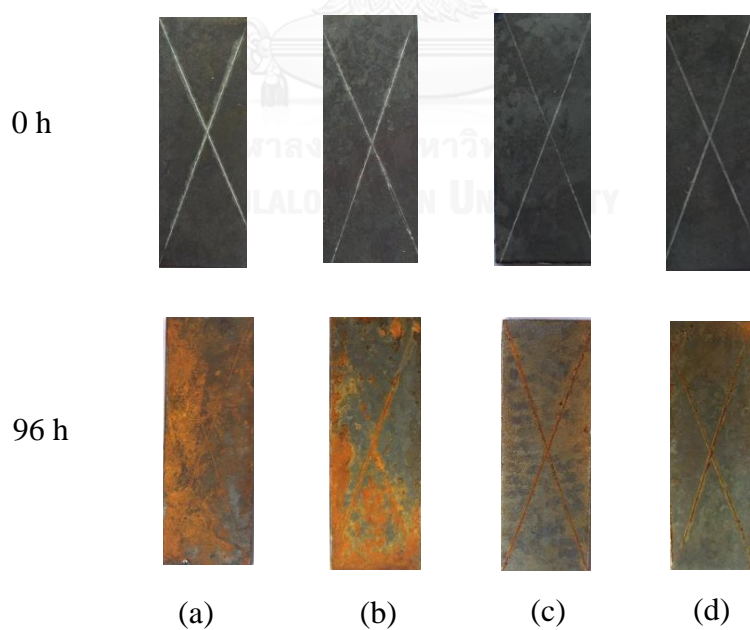


Figure C.2 Coupons of (a) neat TEPA-epoxy, (b) neat *p*-PDA-epoxy, TEPA-epoxy/3wt% untreated silica and (d) *p*-PDA-epoxy/3wt% untreated silica coated on CRS before and after 96 h of salt spray test.

VITA

Mr Saktip kornprasert was born on July 30, 1991 in Bongkok, Thailand. He received his Bachelor's degree of Chemistry, King Mongkut's University of Technology Thonburi (KMUTT). He was admitted to Master Degree in the Program of Petrochemistry and Polymer Science, Chulalongkorn University as student in 2013 and finished his study in 2016.

Presentation at the PCT 6 conference

"Epoxy/modified silica/nanocomposite for anticorrosion", June 30-July 1, 2016, The International Polymer Conference of Thailand 2016 (PCT 6), Bangkok, Thailand.

